FEASIBILITY STUDY ON HIGHLY SLENDER CIRCULAR CONCRETE FILLED TUBES UNDER AXIAL COMPRESSION

Pragati Mysore Paramesh

Thesis submitted to the faculty of the Virginia Polytechnic Institute and State University in partial fulfillment of the requirements for the degree of

Master of Science

In

Civil Engineering

Roberto T. Leon, Committee Chair

Ioannis Koutromanos

Matthew H. Hebdon

6th December 2016

Blacksburg, VA

Keywords: Local buckling, slender, concrete filled tubes, high strength

FEASIBILITY STUDY ON HIGHLY SLENDER CIRCULAR CONCRETE FILLED TUBES UNDER AXIAL COMPRESSION

Pragati Mysore Paramesh

ACADEMIC ABSTRACT

Circular Concrete Filled Tubes are gaining importance in the construction industry due to their advantages insofar as economy and structural efficiency. Due to the recent developments in concrete and steel technology, the usage of high strength materials in these concrete filled tubes is increasing. The governing American specification (AISC 360-16) classifies these composite members as compact, non-compact and slender sections. The allowed section slenderness (ratio of diameter to thickness ratio) in each classification is related to the material properties (ratio of Young's modulus to yield strength ratio). AISC 360-16 is applicable for steels up to 75 ksi and concretes up to 10 ksi. These limits are lower than current available materials and restricts the usage of highly slender sections. As the strength of these tubes is dependent on local buckling, tests on many combinations of high strength steel and concrete are needed to extend these material limits.

This preliminary research work focuses on understanding the local buckling behavior of highly slender sections and the effect of concrete infill and its confinement. The research began by compiling a database that highlighted a gap on tests with highly slender sections and high strength materials. To address this issue, a pilot set of experimental tests were conducted on short circular concrete filled members. An analytical evaluation of these experimental results are performed

using 3D finite element analysis models. The critical buckling load is determined using J_2 deformation theory, which proves to give a good estimate when compared with the experimental results. The main objective of the work is to determine if a simplified test like the one used in this work could be used for the large experimental study that will be necessary to expend the material limits in AISC 360-16. The limited data developed in this study indicates that the test can provide satisfactory results with a few improvements and refinements.

FEASIBILITY STUDY ON HIGHLY SLENDER CIRCULAR CONCRETE FILLED TUBES UNDER AXIAL COMPRESSION

Pragati Mysore Paramesh

GENERAL AUDIENCE ABSTRACT

A concrete-filled tube consists of a large steel circular or rectangular tube filled with concrete. This configuration is widely used in the construction industry, primarily as columns in high-rise buildings. Concrete filled tubes make the best use of both its constituent materials. The strength of the concrete in compression is increased by the confining action of the exterior steel tube, while the relatively thin steel tube is prevented from buckling by the presence of the concrete. Thus, this combination of the two materials, known as composite construction, results in a stronger and more ductile structural member than either a steel only or a reinforced concrete one. The design of these members is currently governed by the American Institute of Steel Construction Manual and Specification known as AISC 360-16. The provisions therein contain specific limits on the strength of both the steel and concrete allowed, as well as on the slenderness (wall thickness to width or diameter) of the tubes permitted. Because stronger steel and concretes are coming into the market and more slender tubes are available, the provisions need updating. This thesis presents a first step in that direction by testing some very slender concrete filled tubes in pure compression.

This thesis presents preliminary research work focused on understanding the local instability of thin walled steel tubes and its effect with a concrete infill. The research began by compiling a database of experimental tests on concrete filled tubes. This database highlighted a gap on test results for thin walled tube sections and high strength materials. To address this issue, a pilot set

of experimental tests were conducted on short circular concrete filled members. An analytical evaluation of these experimental results was performed using 3D finite element analysis models. The test results and accompanying analyses indicate that simplified test like the one used in this work could be used for the large experimental study that will be necessary to expend the material limits in AISC 360-16. The limited data developed in this study indicates that the test can provide satisfactory results with a few improvements and refinements.

ACKNOWLEDGEMENTS

I express my sincere gratitude and appreciation to my thesis advisor Dr. Roberto T. Leon for providing me the opportunity to work on this research and for his encouragement, invaluable guidance and support throughout my graduate studies at Virginia Tech. I am very grateful to Dr.Ioannis Koutromanos and Dr. Matthew H. Hebdon for serving as members of my committee and for providing their insights and critical assessment.

I extend my sincere appreciation to David Mokarem, Brett Farmer and Dennis Huffmann for their assistance with the experimental work. I am grateful for the facilities at Thomas M. Murray Structural Engineering Laboratory at Virginia Tech.

Finally, I express my love and profound gratitude to my parents for providing me with unfailing support and continuous encouragement throughout my years of study and through the process of researching and writing this thesis.

TABLE OF CONTENTS

LIST OF TABLES

LIST OF FIGURES

CHAPTER 1. INTRODUCTION

Steel and concrete are the most common construction materials in the industry and have remained the dominant materials in construction over many years. Concrete possesses excellent axial compressive load carrying capacity, while steel possesses good tensile properties. These characteristics make them perfect materials to withstand the compressive and tensile forces in columns and beam-columns in multi-story structures. Advances in materials technologies have resulted in new high-strength and high-performance concretes and steels, whose combination can results in effective composite steel-concrete members. In particular, innovative concrete filled tubes are now replacing the long established reinforced concrete columns and steel. This thesis explores the feasibility of using a very simple test configuration to conduct the necessary fundamental work that will be required to allow the use of advanced materials in composite members.

1.1 Concrete Filled steel Tube (CFT) members

Concrete-filled steel tubes (CFTs) are composite members consisting of a rolled or built-up structural steel shape or hollow structural section (HSS) with a concrete infill. These members are extensively used in the construction of high-rise buildings and bridges. Due to the simplicity of construction, CFTs are also finding their way into retrofitting for strengthening concrete columns. Watson and O'Brien (1990), for example, found CFTs to be an economical alternative to conventional steel and concrete columns. The interaction between the steel and concrete helps to both delay local buckling of the steel tube and increase the strength of circular CFTs, as well as to

increase ductility in rectangular CFTs due to the confining effect from the steel tube. Schneider (1998) studied a set of short, axially loaded concrete-filled steel tubes and demonstrated that the circular tubes offer substantial post-yield strength and stiffness compared to square or rectangular sections. The CFT cross-section configuration optimizes the strength and stiffness of the member. CFTs eliminate the need for permanent formwork, thereby reducing the construction time.

Webb and Peyton (1990) have shown that using high strength concrete infill with thin walled steel tubes for CFTs results in smaller member sections which provides more rentable space in a building. The behavior of high strength concrete infill exhibits a rapid unloading response in the post-ultimate region with strain reversal, which is evident at strengths of 115 MPa (O'Shea and Bridge, 1994). Thin-walled circular hollow sections under compressive loading are often governed by local buckling capacity, and the strain compatibility between the materials needs to be carefully considered when using high strength concrete.

1.2 American specifications

The Steel Construction Specification (AISC/ANSI 360-16) provides a section classification for composite steel-concrete members subjected to compression and flexure. The circular concrete filled tubes are classified as compact, non-compact, or slender based on the slenderness ratio λ (diameter to thickness or D/t ratio), the steel yield stress (F_y), and the modulus of elasticity of the steel tube (E). These section classifications are available for members subjected to axial compression and flexure (Table 1.1). Currently in the code, the limiting value applicable for steel is up to 75 ksi. There is also a limitation of 3 ksi to 10 ksi for infill concrete strength. The current specification, whose provisions for composite columns were completely revamped in the 2005 edition, gives an accurate prediction of the strength for CFT and encased sections when using its

most detailed analysis method. Predictions using the other more simplified approaches in AISC 360-16 result in generally conservative results.

Table 1. 1 Section classification of Round HSS members (AISC 360-2016)

Description of the element	Width to thickness ratio	λ_p compact/ noncompact	λ_r noncompact/ slender	Maximum permitted
Composite members subjected to axial compression				
Round HSS	D/t	$(0.15E/F_y)$	$(0.19E/F_y)$	$(0.31E/F_y)$
Composite members subjected to flexure				
Round HSS	D/t	$(0.09E/F_y)$	$(0.31E/F_y)$	$(0.31E/F_y)$

1.3 Background and motivation

Composite members have been in use for many years and are gaining more popularity in the construction industry, as the industry is aiming to provide more economical solutions. These economies could be improved by using slender lightweight members and high strength materials. However, the composite behavior of these members is not very well understood as the interaction between the steel and concrete is quite complex. In particular, there is limited knowledge regarding composite filled tubes with high slenderness walls and high strength materials. The

behavior of CFTs depends on the stress-strain behavior of the composite material and their chemical adhesion, friction, and volumetric behavior, which is often difficult to obtain. Hence, understanding the interaction between the steel and concrete, the confinement of concrete core inside steel tube, the local buckling of steel tubes with high slenderness, the scale effect of the members, and the fire resistance have all become major research topicss in the industry.

An initial study based on several existing experimental databases revealed gaps in the databases for tests on high strength materials (concrete and steel) and high cross-section slenderness. Since most experiments have been performed on compact and non-compact sections, very few test data are available for specimens failing in local buckling. A need for continued experimental work in high-strength slender steel tubes infilled with high strength concrete is the main motivation of this research work.

The strength of infill concrete is limited to the range of 3 ksi to 10 ksi in the design of concrete filled tubes (AISC 2010). However, the influence of the strength of concrete (f_c') is not considered directly in computing the section slenderness limit. Concrete, which is very good in withstanding compressive stresses, plays a major role when used in column members and thus it would appear that its properties need to be considered in design, particularly as the ductility and dilatational behavior of the concrete decrease with increases in strength beyond concrete strengths of 100 MPa or so. A reliable analytical model, validated by comprehensive experimental work, is essential. This model will save time and money on performing additional experiments. Thus, new methods need to be developed and validated in order to predict the buckling load of CFTs. Thus the main motivation behind this research is to develop a simple experimental setup which is useful to run large scale experimental parametric study.

1.4 Approach

- A thorough review of the available literature related to the local buckling of circular concrete filled tubes has been completed. As a result of deficiencies in the current research, a strong need for research in this particular field has been demonstrated. The tube sections available on the market are mostly compact. Local buckling was observed but was not found to be the governing failure mode on testing short columns. Very few experiments on steel duct pipes with a yield stress of 60 ksi and thickness of 0.01 inches were performed. Due to the difficulties in fabrication of thin tubes, as well as the lack of availability of slender HSS sections, steel tubes using metal sheets of gages 20 to 24 were fabricated in this research. This method was the best and most feasible option available. Experiments on hollow steel tubes and concrete filled tubes are performed to better understand the local buckling modes. Two configurations of concrete filled tubes have been tested which could be used in the future experimental work.
- A 3D finite element model is developed in order to simulate the behavior of the concrete filled tubes tested. A theoretical evaluation of the critical buckling mode of the column is performed in order to verify the approach, so that the model will be validated and can be used in future work.

The main objective of the work is to determine if a simplified test like the one used in this work could be used for the large experimental study that will be necessary to expend the material limits in AISC 360-16.

1.5 Thesis Organization

Chapter 1 gives some background on concrete filled tubes and its application in the industry. Although this type of column structure has been prevalent in the industry of several years, little is understood about its behavior due to its composite nature. The motivation for this research and the approach to tackle this problem is also outlined in this chapter.

Chapter 2 investigates the need for experimental work on highly slender CFTs by identifying the gaps in the available database.

Chapter 3 details the experimental part of this research, which consisted of testing built-up steel tubes under axial compression with and without infill. The details of the type of specimen used for testing, material properties, the applied load and the end restraints, and the test setup are presented. The test results for both the hollow tube and the concrete filled tube testing are explained. Sources of error and uncertainties associated with the testing are detailed in this chapter.

Chapter 4 focuses on the analytical prediction of the test results using a finite element model. The circular concrete filled tube and the hollow tube are modeled following the procedure outlined in this chapter. The load-axial shortening curve for static loads is obtained, and this curve should be directly comparable to the experimental tests results.

Chapter 5 deals with a theoretical approach followed to predict the critical local buckling loads for hollow tubes the concrete filled tubes. The theoretical approach is based on the J_2 deformation theory. This theory provides better estimates of plastic buckling loads, which is a limit state relevant for concrete filled tubes.

In chapter 6, the results obtained from the experiments, analytical models and theoretical predictions are compared and results are assessed. This is necessary to validate the finite element model and use the theoretical procedure for future tests on similar specimens.

Chapter 7 summarizes the results obtained from the experimental, analytical and theoretical approach. The uncertainties involved in obtaining the perfect (absence of initial imperfection) buckling mode and the actual maximum buckling load is discussed. The need for future work in this field and the procedure to follow is mentioned in Chapter 8. It also gives an idea on how the tests could be modified to obtain more accurate results.

CHAPTER 2. LITERATURE REVIEW

2.1 Experimental database

Thousands of experiments have been conducted on CFT columns and beam-columns (Leon et al, 2012). Most of the experiments have limitations with regards to the slenderness ratio and the strength of materials used. Very few experiments look into failure through local buckling. A database has been established by gathering the test results from experiments performed by researchers like Bridge & O'Shea (1997 & 2000), Yoshoika et al (1995), Nakahara & Sakino (1998), Varma (2000), Leon et al (2012), Inai & Sakino (1996), Fujimoto et al (1995), Nakahara (2000), Uy (2000), Janss (1974), Schneider (1998), and Mursi et al (2003). This database includes tests on compact, non-compact, and slender CFT columns and beam-columns subjected to axial forces and flexure and failing in local buckling. The database contains tests performed on CFTs with a minimum strength of 8 ksi for concrete and 60 ksi for steel. The specimens have a wide range of depth to thickness ratios (D/t or h/t) ranging from 20 to as high as 200.

2.1.1 Experimental Tests of CCFT members

A total of 373 test data is available for Circular Concrete Filled Tubes (CCFT), which includes 272 column tests and 101 beam column tests, meeting the material limits discussed above. A summary of the CCFT database has been extracted and is shown in Table 2.1. The frequency distribution graph in Figure A.1 and Figure A.3 shows the number of specimen data available, while Figure A.2 and Figure A.4 illustrates the number of specimens failing in local buckling for varying strengths of steel and concrete. From Figure A.8, one can observe that there are very few test data available for members with both high strength concrete and steel failing in local buckling.

Figure A.5 and Figure A.6 show the strengths of concrete and steel, as well as the D/t ratios of the members. The data points towards the center of the plot belong to members with high strength materials. Table 1.1 shows the classification mentioned in AISC 360-16. To understand the section classification of the test specimens, normalized D/t scatter plots are shown in Figures A.9 to A.18. A D/t value of 1.0 indicates the normalized upper and lower limiting value (λ). The data points above the line indicate sections above the lower limit, while the data points below the limit line indicate the sections below the upper limit.

Table 2. 1 Database of CCFT members

CCFT member Type	Column			Beam Column	
Section classification	Compact	Non-compact	Slender	Compact	Non-compact
Total number of tests	284	26	27	90	41
Number of tests failing in local buckling	0	20	22	0	6
Minimum Fy (ksi)	33.6	26.8	30.6	27.5	26.9
Maximum Fy (ksi)	121	83.9	121	66.7	70
Minimum fc' (ksi)	3.5	4	3.5	5	4.5
Maximum fc' (ksi)	10	12	16	16	15
Minimum D/t	13.8	52.4	52	12.8	73.5
Maximum D/t	125	168.1	220.9	73.5	220.9

2.2 Research on CCFT members

There are several analytical and experimental research efforts performed on circular concrete filled tubes that are relevant to this research. The following subsection gives a brief description of some of those efforts.

2.2.1 Cross sectional slenderness limits

Bradford et al (2002), performed a theoretical study on local and post-local buckling of thin-walled circular steel tubes with a rigid infill. The main motivation was the investigation of cross sectional behavior of CFTs. Both analytical and experimental work were considered in this research work. One of the main findings was that the infill in the steel tubes not only enhances the cross sectional properties but also delays the buckling of the steel tube. In this paper, cross section slenderness limit is proposed for the buckling strength which was the initial intention of this research work. The theoretical model uses Rayleigh-Ritz approach to determine the minimum elastic buckling stress which is show in Eq. 2.1.

$$\sigma_{ol} = \frac{2E}{\sqrt{(1-\nu^2)}} \frac{1}{(d/t)} \qquad \text{(Eq. 2.1)}$$

In Eq. 2.1, E is the Young's modulus, ν is the Poisson's ratio, d is the diameter of the tube and t is the thickness of the tube. The modified slenderness ratio is given in Eq. 2.2

$$\lambda_e = \left(\frac{d}{t}\right)\left(\frac{Fy}{250}\right) \qquad \text{(Eq. 2.2)}$$

F_y is in units of N/mm^2 and 250 is the representative yield strength for steel. The cross section is considered to be fully effective when $\lambda_e \leq 125$ and slender when $\lambda_e > 125$. This is based on the best

curve fit in the calibration procedure and is greater than that for a hollow CHS section for which the slenderness limit is $\lambda_e = 100$ which is suggested by Bradford et al (2001). It was also derived that the elastic buckling stress is $\sqrt{3}$ times that of its unfilled counterpart which was based on the Rayleigh-Ritz method.

2.2.2 Local buckling of CFT

Local buckling of short, circular thin-walled concrete filled tubes was analyzed by O'Shea & Bridge (1997). Two major possible failure modes were identified: local buckling and yield failure. Some important conclusions of their research were that the failure modes are independent of the diameter to thickness ratio, but were dependent on the bond between the steel and concrete infill. Since there was less data available for thin steel tubes, experimental evaluation was undertaken. Ten axially loaded tubes with varying D/t ratios from 58.6 to 220.4 and with a length (L) to diameter (D) ratio of 3.5, which falls in the short column category, were tested. The steel tube used for this experiment has a normal yield strength of 185 MPa to 363 MPa. Figure 2.1 shows the normalized load-shortening response for varying slenderness ratios. In the yield failure, the principal strains increased with axial shortening strain, whereas in buckling failure, the bond between concrete and steel tube was not maintained, leading to the sudden change in the slope of the curve (Figure 2.1 a). The significant improvement in the strength and ductility of nominal strength (50 MPa) concrete was observed to be a result of the confining action of thin-walled circular steel tubes compared to high strength (80 MPa) concrete, where the ductility improved for thicker tubes. This characteristic can be observed in Figure 2.1 c and Figure 2.1 d. Where f_y is the steel yield strength determined by tensile coupon testing, f_{test} is the experimentally applied stress

on hollow specimens, *fc* is the concrete compressive strength and f_{cc} is the peak confined concrete compressive strength.

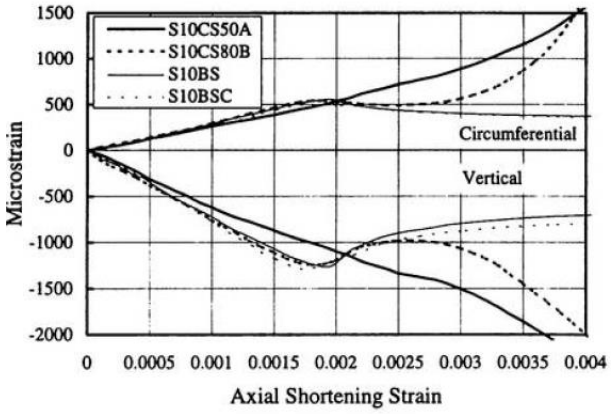

Figure 2.1 a Local strains for BS (unfilled) and BSC (filled) specimens

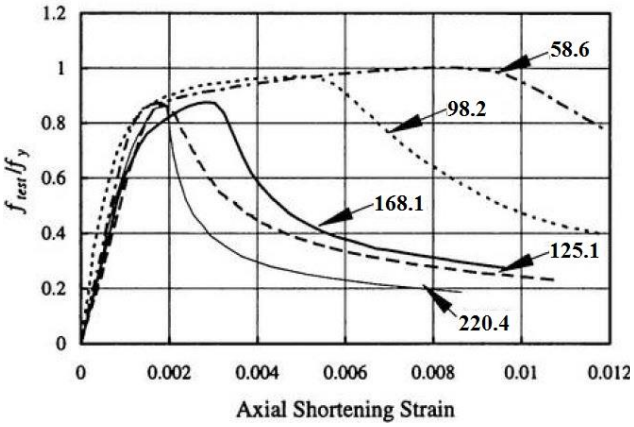

Figure 2.1 b Normalized load axial shortening response for unfilled steel tubes

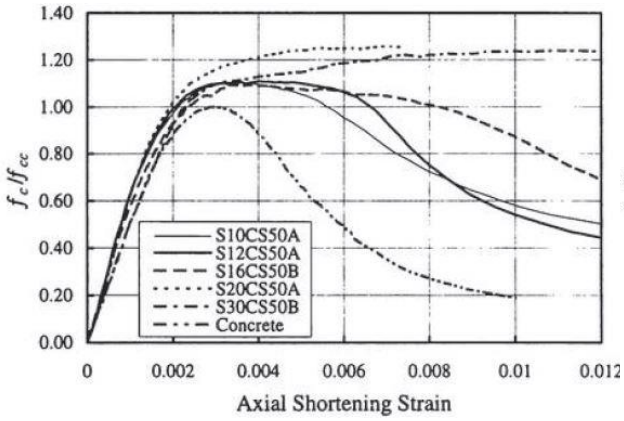

Figure 2.1 b Confined concrete response for nominal 50 MPa mix

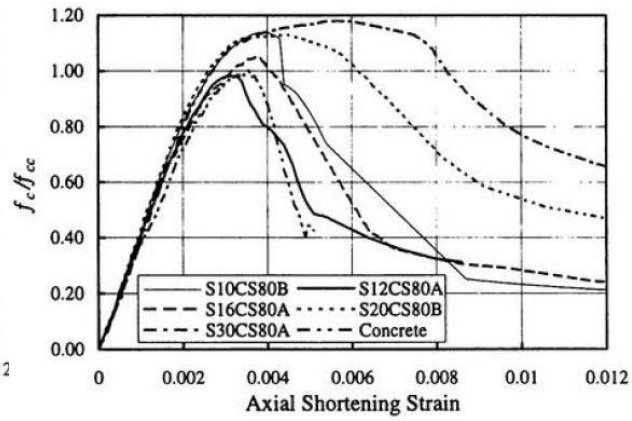

Figure 2.1 d Confined concrete response for nominal 80 MPa mix

2.2.3 Behavior of axially loaded concrete-filled steel circular stub column

Ellobody et al (2006) performed an extensive study over a range (30 to 110 MPa) of concrete strength in concrete filled tubes under axial compression. The cross-section slenderness (D/t) of the tubes studied ranged from 15 to 80, which included compact tubes section. A finite element

program ABAQUS was used to develop an accurate analytical model. The results from these analysis were verified with the tests conducted by Giakoumelis and Lam (2004) and Sakino et al (2004).

The confined concrete, steel tube, and interface between the two were carefully modeled by selecting an appropriate element type and mesh size to yield accurate results with reasonable computational time. It was found that a mesh size of 1:1:2 (length:width:depth) can achieve accurate results for most elements. The top and bottom surfaces were fixed in all degrees of freedom except the displacement at the top surface in the direction of application of load. Load increments were applied using the RIKS method in the ABAQUS library, since this method is used to predict non-linear collapse, such as post-buckling analysis. A static uniform load was applied using displacement control at each node of the top surface. For the material model, two multi-linear stress-strain curves were used. Young's modulus was 205 GPa, and Poisson's ratio was taken to be 0.3 for steel. The strength of the confined concrete was determined using the equation proposed by Mander et al (1988). Young's modulus was calculated using the empirical equation given by ACI 318-14, and Poisson's ratio was considered to be 0.2. The Drucker Prager model in ABAQUS was used to model the confined concrete, while the interface between the steel and concrete was modeled by interface elements. The coefficient of friction between the two faces was taken to be 0.25 for the analysis.

A comparison between the experimental results and finite element results was conducted to verify the finite element model. The ultimate load and load-axial shortening curves, as well as the

deformed shapes were also investigated. The experimental and analytical results agreed well within reason. The plots of load-axial shortening curves for the columns without concrete infill are shown in Figure 2.2 a. It can be observed that the finite element model accurately predicted the ultimate load of the columns and the load-axial shortening behavior. Figure 2.2 b illustrates the plots of axial shortening for concrete filled tubes specimens. The predicted column strength using the finite element model was 7% greater than the experimental results. A parametric study of 40 circular concrete filled compact tubes with varying D/t ratio (15 to 70) and varying strength of infill concrete (30 to 110Mpa) was performed using finite element analysis. The results from this exercise demonstrated that the American specifications are conservative. However, they are capable of producing reliable limit state design when a resistance factor of 0.85 is used for axially loaded concrete filled tubes.

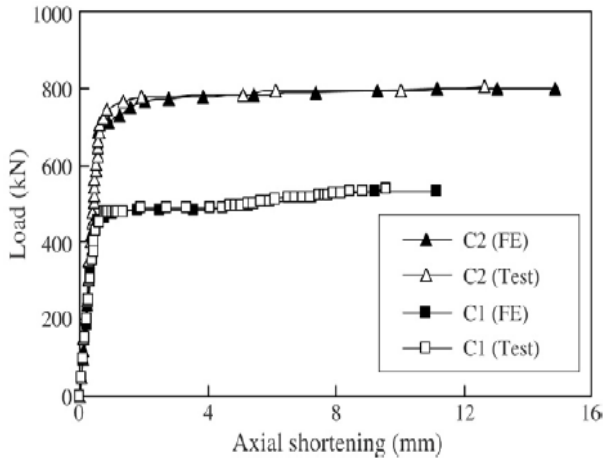

Figure 2.2 a Comparison of experimental and finite element analysis load-axial shortening curves for tubes without infill

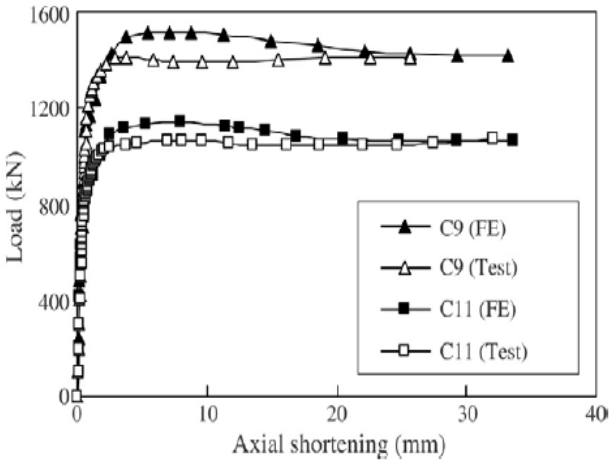

Figure 2.2 b Comparison of experimental and finite element analysis load-axial shortening for tubes with concrete infill

2.2.4 Elastic and plastic buckling of cylindrical shells with elastic core

The elastic and plastic buckling of circular cylindrical shells with rigid core materials under axial compression was analyzed by Zhang J (2009). Some assumptions made to better analyze an infinitely long cylindrical shell are as follows: 1. The shell is geometrically perfect, 2. It is made of an isotropic material, 3. The self-weight is negligible, 4. It is loaded uniformly in the longitudinal direction, 5. The boundary of the shell remains perfectly circular under loading and buckling, and 6. The shell buckles when the critical stress is reached. The buckling considered is of the bifurcation type. The elastic infill that forms a core requires no additional effort to create a bond with the surrounding shell, thereby making it incapable of resisting the tensile or frictional forces. However, the core provides compressive resistance to inward movement of the shell, and the buckling of the shell under this constraint is called one-way-buckling. The compressive reaction forces are assumed to be proportional to the radially inward deflections.

The governing equations are derived using the virtual work method. Bifurcation occurs at the compressive stress, σ_{cr}, and the reference geometry is considered just before the bifurcation. An elastic bifurcation buckling for a hollow shell is given by Eq 2.3, where N_{cr} is the minimum critical load, R is the radius of the tube, t is the thickness of the shell, E is Young's modulus, and ν is Poisson's ratio.

$$N_{cr} = \frac{Et^2/R}{\sqrt{3(1-\nu^2)}} \qquad \text{(Eq. 2.3)}$$

The above expression is identical to the equations given by Timoshenko and Gere (1961). With a rigid core (k = ∞), the buckling load increases by 5/3 times that of hollow shell (k = 0) which is given in Eq. 2.4 and, the buckling wavelength is given by Eq. 2.5.

$$N_{cr} = \frac{5}{3}\frac{Et^2/_R}{\sqrt{3(1-\nu^2)}} \quad \text{(Eq. 2.4)}$$

$$l = \sqrt{3}\frac{\pi\sqrt{Rt}}{\sqrt[4]{12(1-\nu^2)}} \quad \text{(Eq. 2.5)}$$

The elastic bifurcation buckling load for shell with a varying foundation modulus is given by Eq. 2.6 where α, β and γ are buckling parameters defined in the Table 2.2. α is defined as equal to N_{cr}/N_{cro}, which is the ratio of the buckling load value of hollow shell. β is defined as the upper bound and equal to ξ/l_o, while γ is equal to ζ/l_o. 2ζ and 2ξ are the contact and no-contact buckling wavelengths. Buckling wavelength is furthermore given by Eq. 2.7.

$$N_{cr0} = \frac{Et^2/_R}{\sqrt{3(1-\nu^2)}} \quad \text{(Eq. 2.6)}$$

$$l_o = \frac{\pi\sqrt{Rt}}{\sqrt[4]{12(1-\nu^2)}} \quad \text{(Eq. 2.7)}$$

Table 2. 2 Buckling parameters for infinitely long shells with different foundation moduli

	$k = 0$	$k = 10$	$k = 100$	$k = 1.0 \times 10^6$	$k = \infty$
α	1	1.320	1.629	1.667	1.667
β	0.5	0.691	0.859	0.866	0.866
γ	0.5	0.441	0.010	0.003	0

It can be observed that with the increase in the foundation modulus value, the buckling load and the no-contact wavelength increases to a limit of 1.667 and 0.866, respectively. However, the contact wavelength decreases to zero. The influence of the foundation modulus *k* on the buckling load is also shown graphically, which can be obtained using *Mathematica.*

The plastic bifurcation load of a shell with a hollow core is given by Eq. 2.8. The buckling wavelength *l* at the bifurcation buckling load is given by Eq. 2.9, where *B, C',* and *D'* are constants as defined below. The two parameters in the constants' equations are given by $e = E/E_s$ and $\lambda = E/E_t$, where $E_s = \sigma/\varepsilon$ is the secant modulus, and $E_t = d\sigma/d\varepsilon$ is the tangent modulus obtained from a uniaxial stress-strain curve of the material at the stress level equal to the applied axial stress.

$$B' = \frac{E(\lambda + 3e + 3)}{\lambda(5 + 3e - 4\vartheta) - (1 - 2\vartheta)^2}$$

$$C' = \frac{2E(\lambda - 1 + 2\vartheta)}{\lambda(5 + 3e - 4\vartheta) - (1 - 2\vartheta)^2}$$

$$D' = \frac{4E\lambda}{\lambda(5 + 3e - 4\vartheta) - (1 - 2\vartheta)^2}$$

$$N_{cr} = \frac{t^2}{R}\sqrt{\frac{(B'D' - C'^2)}{3}} \qquad \text{(Eq. 2.8)}$$

$$l = \pi\sqrt{Rt}\sqrt[4]{\frac{B'^2}{12(B'D' - C'^2)}} \qquad \text{(Eq. 2.9)}$$

The plastic bifurcation load of the shell with a rigid core is given by Eq. 2.10. The buckling wavelength of the tube with rigid core is given by Eq. 2.11. It can be observed that the buckling

load for shell with rigid core is 5/3 times that of hollow shell and the buckling wavelength of shell with rigid infill is √3 times that of hollow cylindrical shell.

$$N_{cr} = \frac{5}{3}\frac{t^2}{R}\sqrt{\frac{(B'D' - C'^2)}{3}} \quad \text{(Eq. 2.10)}$$

$$l = \sqrt{3}\pi\sqrt{Rt}\sqrt[4]{\frac{B'^2}{12(B'D' - C'^2)}} \quad \text{(Eq. 2.11)}$$

The plastic buckling of an elastic core with varying foundation moduli is similar to the case of elastic buckling, with the only difference being that the modulus of elasticity is now dependent on the stress and not the constants, as used in the case of elastic buckling. The buckling parameters were not derived for the plastic case, since they are material dependent, and a general plot cannot be obtained. However, it is experimentally observed to follow the same trend as the elastic buckling parameters.

A verification of the theoretical analyses was performed using the most practical application of concrete filled tubes. The theoretical results were compared to experimental results of Sakino et al, O'Shea and Bridge, and Lam and Gardner. It was observed that the theoretical predictions were in good agreement and are less conservative compared to Eurocode and CSA.

2.3 Material stress-strain curve

The stress-strain curves are approximated by using the analytical expression (Eq. 2.12) proposed by Ramberg and Osgood (1943). This formula describes the stress-strain curve in terms of three parameters: Young's modulus and two secant yield strengths.

$$\epsilon = \frac{\sigma}{E} + K\,(\frac{\sigma}{E})^n \quad \text{(Eq. 2.12)}$$

$$K = \epsilon_y(\frac{E}{\sigma_y})^n \quad \text{(Eq. 2.13)}$$

In Eq. 2.12, σ and ϵ are the stress and strain values respectively, and E is Young's modulus. The value of the constant K is given by Eq. 2.13, where ϵ_y is the yield strain corresponding to yield stress σ_y. Finally, *n* is the shape parameter, which is given by Eq. 2.14:

$$n = 1 + \frac{0.3853}{\log_{10}\frac{\sigma_1}{\sigma_2}} \quad \text{(Eq. 2.14)}$$

Where σ_1 is the first secant yield strength corresponding to secant modulus m_1E, and σ_2 is the second secant yield strength corresponding to secant modulus m_2E. The constants m_1 and m_2 are equal to 0.7 and 0.85 respectively. The value of m_1 is obtained by considering a 0.2-percent offset in yield strength, and m_2 is chosen such that it lies between 0.7 and 1.0 and is on the safe side of the limiting value of m = 0.9.

The tangent modulus at a given stress is the slope of the tangent at that stress in the stress-strain curve. The ratio of Young's modulus to the tangent modulus is given by a dimensionless equation as shown in Eq. 2.15.

$$\frac{E}{E'} = 1 + \frac{n(1-m_1)}{m_1}(s)^{n-1} \quad \text{(Eq. 2.15)}$$

The tangent modulus *E'* is determined using $m_1 = 0.7$. The constant *s* is the stress ratio equal to $\sigma/\sigma_{1.}$ The value of stress σ should be carefully chosen, since it determines the capacity of the member at that stress.

CHAPTER 3. EXPERIMENTAL WORK

A set of experiments were performed on both hollow and concrete filled tubes in order to understand the local buckling behavior in high D/t ratio specimens. A total of 20 specimens with varying D/t ratios were tested; 8 were hollow tubes and the remaining 12 were filled with high strength concrete. These were tested using the United SHFM Servo-Controlled Hydraulic universal testing machine (UTM) having a capacity of 600 kN. The machine is located in 129 Norris and is part of the undergraduate construction materials laboratory at Virginia Tech.

3.1 Material description

3.1.1 Steel tube

The steel tubes were constructed from a thin steel plate rolled to form a tube. To determine the strength of the steel, a set of coupon tests were performed according to ASTM E8-15a *Standard Test Methods for Tension Testing of Metallic Materials*. Tension tests were performed on the coupons to determine the yield stress, ultimate strength and elongation capacity of the steel tube material. An electromechanical INSTRON UTM with a capacity of 600kN was used for the tension testing. Manual wedge action grips suitable for thin flat specimens were used for easy specimen loading, alignment and positioning. The small preload applied by the grips upon tightening was manually removed with the fine position adjustment control available for this UTM. A 50mm extensometer with a suitable clip was attached measure the strain in the specimen up to about 5% strain (see Fig B.1.2). The specimen failure is shown in Figure B.1.3.

The stress strain behavior of the material under tensile testing is reported in Appendix B.1. The summary of average yield stresses of the material is shown in Table 3.1. The Young's modulus results averaged to a nominal value of E_s = 27984 ksi. This value of Young's modulus was used to obtain the parameters for a Ramberg-Osgood curve to be used in the theoretical predictions.

Table 3. 1 Summary of coupon testing

Gauge thickness ga (inches)	Yield stress (ksi)	Ultimate stress (ksi)	Elongation (%)
20	22.1	39.4	24.5
22	22.1	39.4	22.1
26	22.1	39.4	22.7

3.1.2 Concrete infill

The tubes were infilled with concrete. The compressive strength of the concrete was determined using 4x8 standard cylinders which were made at the time of concrete casting. The concrete mix design is detailed in Appendix B.2. A workable concrete mix was produced to avoid concrete segregation and avoid the use of vibrator.

A set of ten cylinders were tested according to ASTM C33 to determine the concrete compressive strengths using a Forney concrete cylinder testing machine. The tests on CFT specimens were performed on the 14^{th} day of casting. The concrete cylinders were tested on the same day as the filled specimens to determine the actual concrete strength at the time of testing. The compressive strengths of concrete (f_c) from the compression testing results are summarized in Table B.2.1.

3.2 Specimen description

The available database has less experimental results for higher D/t ratio. This created a requirement of performing laboratory experiments on specimens with high cross section slenderness. For the most applications of CFTs, HSS sections are used. Due to the limitations on slenderness mentioned in the codes, HSS sections with high D/t ratios are unavailable in the market. Although HSS with high D/t can be fabricated, these type of tubes require special milling and can be procured only in large quantities, which was not feasible for this study. Hence, the tube had to be manufactured by VT personnel and rolling conventional thin steel sheets was the only option. Several types of materials including mechanical duct pipes were looked at. Due to the extremely small thickness it was difficult to work with and weld them together to form a near perfect circular tube. Thus, higher thickness sheets were considered. Steel galvanized sheets of 20ga, 22ga and 24ga were chosen; this material is easy to work with and can withstand spot weld. Unfortunately, high strength metal sheets are not readily available and this research had to focus on normal strength steel.

Twenty steel tubes of 5 inches in diameter and 16 inches in length were fabricated at the Murray Structural Engineering and Materials Laboratory at Virginia Tech. The metal sheets were rolled into tubes using a sheet metal roller; the process required several passes to get the desired diameter. A standard spot welding procedure was followed to weld the tube; thus there was not a continuous weld.

The top and bottom surfaces of the tubes were milled and to ensure that the ends were as flat as possible. Having a uniform plane at the top and bottom surfaces is important to obtain a uniform load application and avoid undesirable initial imperfections in the loading procedure. The details of the specimen and their designations are shown in Table 3.2. In the specimen designation, HST is the Hollow Steel Tube and CFT is the Concrete Filled Tube.

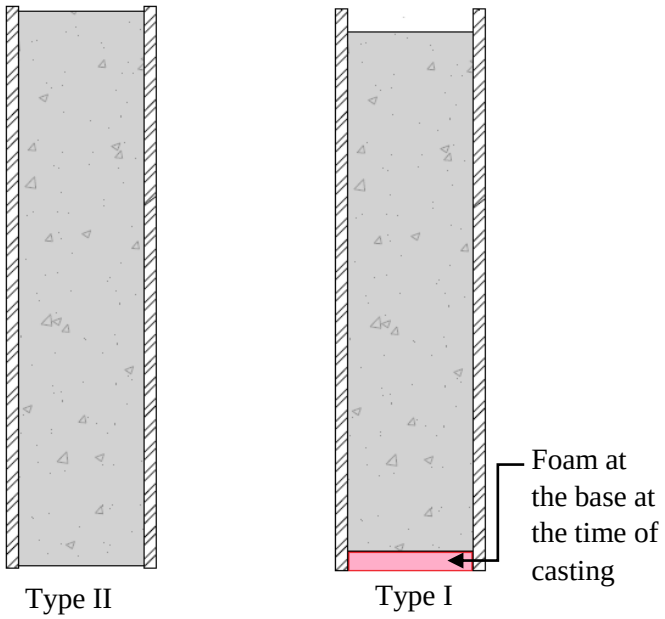

Figure 3. 1 Section view of Type II and Type I CCFT specimen

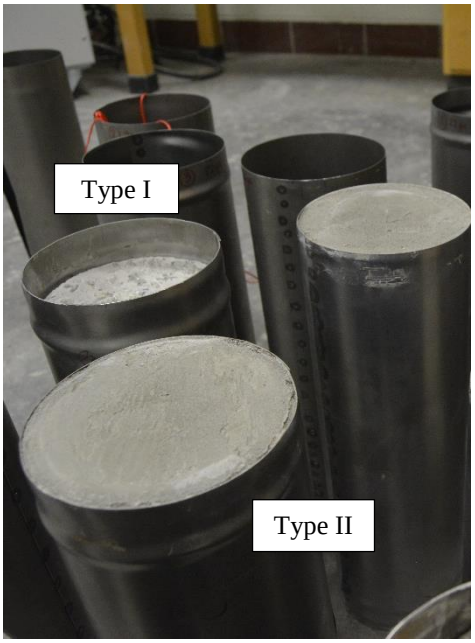

Figure 3. 2 Concrete infill in the CCFT specimens

Two types of concrete filled tubes were prepared (Figure 3.1 and Figure 3.2). Type I had a concrete infill for a depth of 14 inches with a gap of an inch at the top and bottom of the tube. To achieve the gap in the infill, foam material was placed at the bottom of the tube before the concrete was poured and was well packed at the base. These specimens were developed to understand the behavior of the filled tube and to see if the bond between the concrete and the steel contributes to the increase in load carrying capacity.

Type II specimens had concrete infill depth almost equal to the height of the tube. The surface of the concrete was slightly (0.1 in.) below the ends of the steel tube. This ensured that the application of load was on the steel tube alone such that only outward buckling occurred. The application of the load over the concrete surface was avoided since the research is about local buckling and not focusing on getting a higher load carrying capacity.

Table 3. 2 Summary of specimen tested

Specimen designation	Gage (ga)	Measured thickness t (inches)	Specimen Slenderness D/t
20-HST-01	20	0.0392	127.5
20-HST-02	20	0.0392	127.5
22-HST-01	22	0.0325	153.8
22-HST-02	22	0.0325	153.8
22-HST-03	22	0.0325	153.8
22-HST-04	22	0.0325	153.8
24-HST-01	24	0.0241	207.5
24-HST-02	24	0.0241	207.5
20-CFT-I-01	20	0.0392	127.5
22-CFT- I -01	22	0.0325	153.8
24-CFT- I -01	24	0.0241	207.5
20-CFT-II-01	20	0.0392	127.5
20-CFT- II -02	20	0.0392	127.5
22-CFT- II -01	22	0.0325	153.8
22-CFT- II -02	22	0.0325	153.8
22-CFT- II -03	22	0.0325	153.8
22-CFT- II -04	22	0.0325	153.8
22-CFT- II -05	22	0.0325	153.8
24-CFT- II -01	24	0.0241	207.5
24-CFT- II -02	24	0.0241	207.5

3.3 Loading and boundary conditions

The specimens were tested under axial compression. Monotonic loading was applied on all the specimens at the rate of 0.05 in/min. The load on the hollow tubes was applied until failure where the load carrying capacity of the tube reduced significantly due to local buckling. On the other

hand, for the concrete filled tubes the load was applied until local buckling was observed; this was indicated by a slight reduction in the load carrying capacity which picked up once the contact between the platen and the concrete surface was achieved.

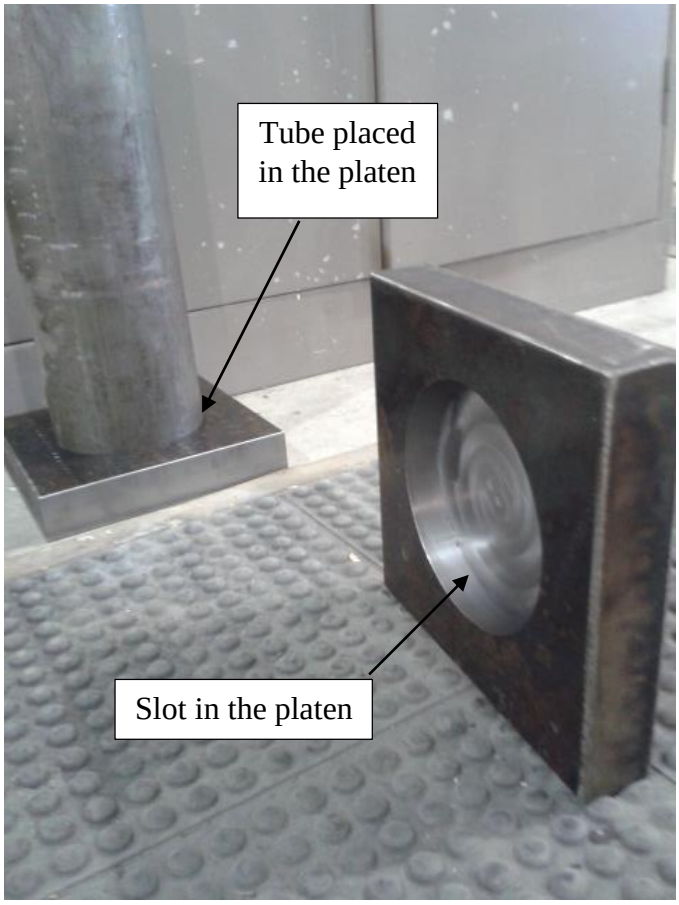

Figure 3. 3 Platen used to restrain the ends of the tube

These tests are performed without introducing any imperfections. Thus the ideal boundary condition for this case is to have both the top and bottom surfaces fixed in all degrees of freedom except the translation at the top surface in the direction of load application. By placing the tubes in the compression testing machine, this type of boundary condition is not achieved since the ends are not restrained in horizontal translation. Hence, two platens were fabricated by creating a slot

in a 1 inch thick steel plate for a depth of about ¾ inches. The slots were perfectly created which allowed the tubes to neatly fit inside without allowing much room for translation.

3.4 Test setup

A typical setup can be seen in Figure B.3.1. The bottom platen is placed exactly at the center of the loading frame with the help of the alignment circles in the UTM surfaces. This ensures that the center of application of the load is in line with the axis of the tube not allowing any eccentricity. They are fixed in place with the help of grips on either side. The tubes were placed over the platen and then the top platen was placed over the tube. The loading head was brought close to the top platen and then the load is applied. These experiments have a fairly simple test setup due to their small size.

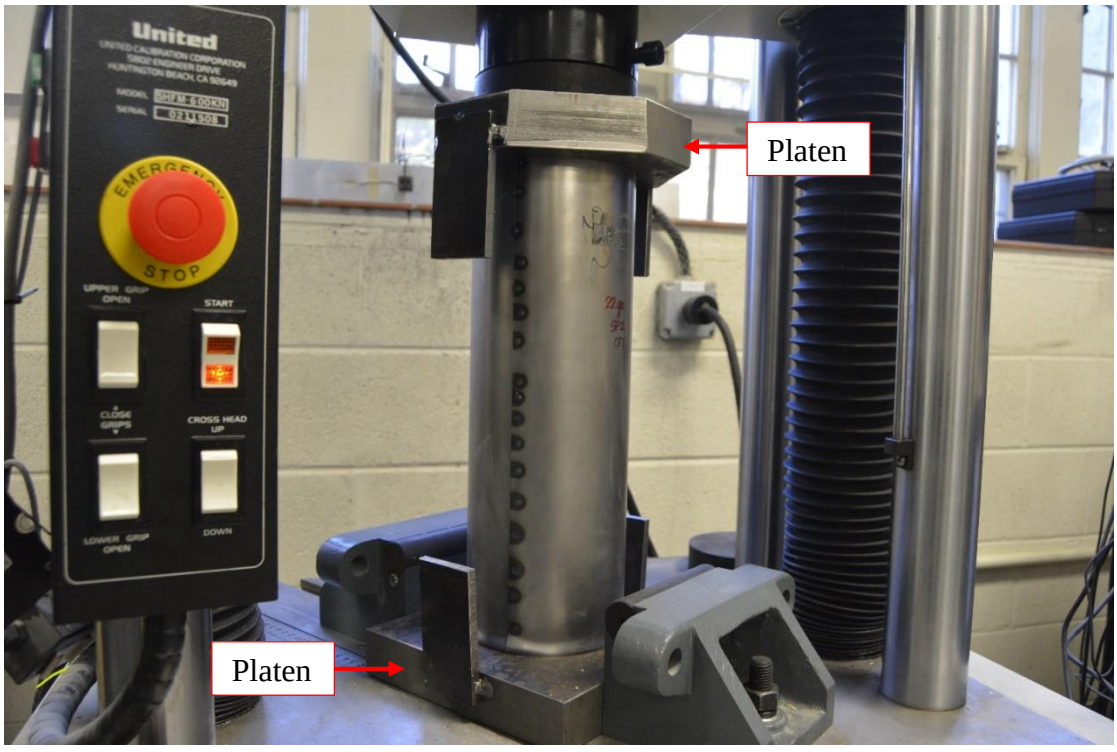

Figure 3. 4 Typical test setup for HST and CCFT compression testing

3.5 Testing of specimens

3.5.1 Measurements

The United UTM does not have a strain device with the diameter that would have been needed for these specimens (125mm). Thus, only the load applied and the axial shortening were recorded. This machine has an interactive interface with the computer which allows one to view the plots as required. The displacement is measured is the position of the cross head. The force is applied at a slow rate of 0.05 in/min and the force in lbs and position in inches are recorded every 0.1 second.

3.5.2 Testing of hollow specimens

The hollow tubes were placed as mentioned in the test setup and a monotonic load was applied slowly. No preloading was applied. The hollow tubes initially remained straight; as the critical load was reached, the specimens started to exhibit local buckling at the top and/or bottom end. The specimen behaved like a shell due to its high slenderness ratio and was bound to fail in local buckling. Multiple buckling waves were observed in most specimens. Since there is no restraint in the core, the tube tends to buckle both inwards and outward causing two-way buckling (see Figure 3.5). The local buckling failure mode of a hollow tube can be seen in the photos in Appendix C. The plots of applied load vs axial shortening (P-Δ) curve for the three different specimens can be seen in Figures 3.1 through 3.3. The buckling load for each specimen and the corresponding displacement is presented in Table 3.3.

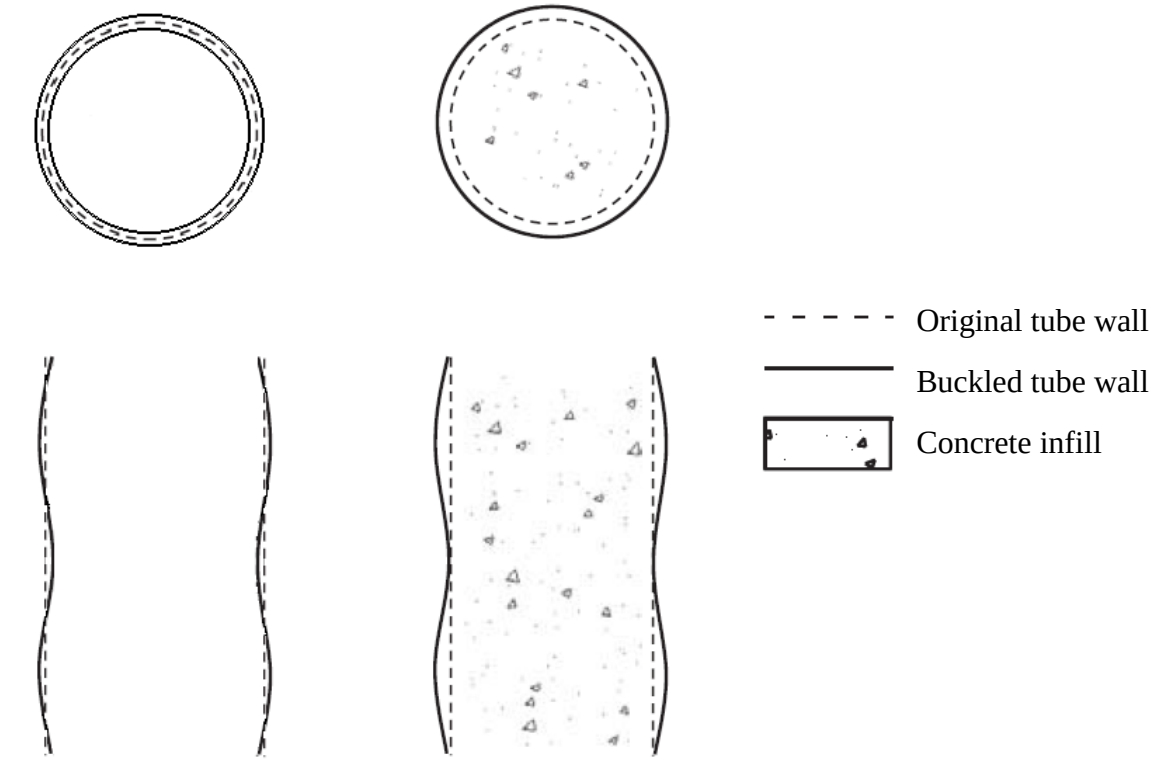

Figure 3. 5 Two way and one way local buckling of hollow tubes and concrete filled tubes respectively

Table 3. 3 Summary of buckling load and axial shortening from hollow tube testing

Specimen	Buckling load (kips)	Axial shortening at buckling (inches)
20-HST-01	14.60	0.065
20-HST-02	13.14	0.060
22-HST-01	10.29	0.063
22-HST-02	9.80	0.055
22-HST-03	8.16	0.06
22-HST-04	10.69	0.053
24-HST-01	4.75	0.040
24-HST-02	7.48	0.035

3.5.3 Testing of concrete filled tubes

The concrete filled tubes were tested under compression. Two types of CFTs were tested. Tests on Type I specimens did not show much difference when compared to the hollow tube testing since the local buckling occurred at the ends of the tube and the ends lacked core restraint. Two wavelengths were typically observed at the ends. One way buckling (Figure 3.5) was seen in the regions where the rigid core restraint was present. Tests on Type II specimens also resulted in local buckling at the ends of the tube. However, the buckling wavelengths were smaller in length and one way buckling was observed throughout. Loss of bond between the concrete and steel tube was also observed. Since the load is applied on the steel tube alone, the compressive strength of concrete does not affect the local buckling failure of the steel tube. A summary of the CCFT test results is shown in Table 3.4. The plots of applied load vs axial shortening of the Type I specimens

can be seen in Figure 3.4. The applied load vs axial shortening for CCFT type II specimens are shown in Figures 3.5 through 3.7. It can be observed that all the specimens failed in local buckling. The deformed shape of the CCFT specimens can be seen in Appendix D.1 and D.2.

The experiments were performed on the short specimens with an L/D ratio of 3. The buckling loads obtained from the experiment involves uncertainties due to imperfection. The imperfections in the specimens are caused due to the following;

- Errors in spot welding: the tubes are fabricated at the laboratory which is made by rolling the metal sheets and welding it. Improper welding leads to errors in the test results. In Figure C.4 the error in spot welding could be observed which caused the tube to open up at the center on loading.
- Non-uniform ends: the tube ends play an important role in distributing the loads. A uniform surface ensures uniform loading and avoids eccentric loading caused due to the improper milling of the ends.
- Out-of plumbness: it is very important to have the centerline of the specimen aligned with the center line of load application. Even the slight error in this causes eccentric loading.
- Material overlap: the tubes are fabricated to achieve sections similar to HSS sections. An overlap of the metal sheet during fabrication of the tube has an effect on the results.
- End restraints: in order to hold the tube ends in place, they are placed in the slots of the platens. Due to minor error in the fabrication, it is difficult to obtain a snug fit in the platens. The local buckling of the steel tube inside these slots are observed during the experiment.

Table 3. 4 Summary of buckling load and axial shortening from concrete filled tube testing

Specimen	Buckling load (kips)	Axial shortening at buckling (inches)
20-CFT-I-01	13.84	0.060
22-CFT- I -01	9.42	0.050
24-CFT- I -01	5.54	0.035
20-CFT-II-01	14.31	0.050
20-CFT- II -02	13.25	0.060
22-CFT- II -01	11.00	0.067
22-CFT- II -02	11.70	0.055
22-CFT- II -03	10.37	0.050
22-CFT- II -04	14.99	0.060
22-CFT- II -05	12.50	0.053
24-CFT- II -01	5.97	0.054
24-CFT- II -02	6.50	0.035

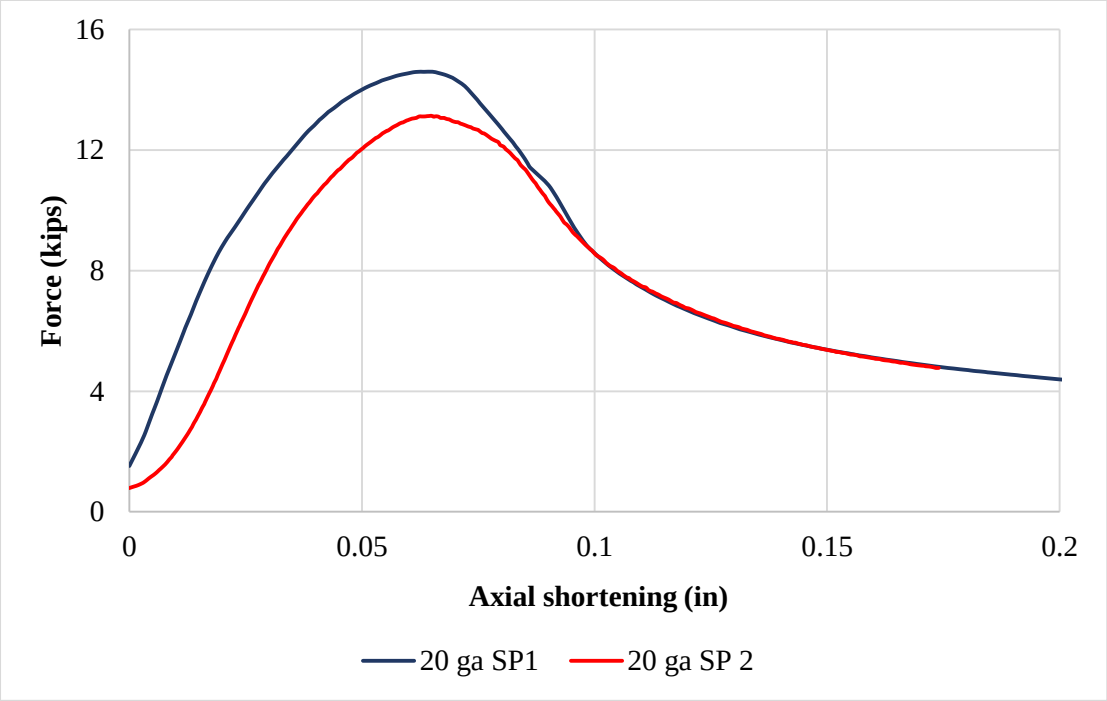

Figure 3. 6 Applied load- axial shortening curve obtained from 20ga HST testing

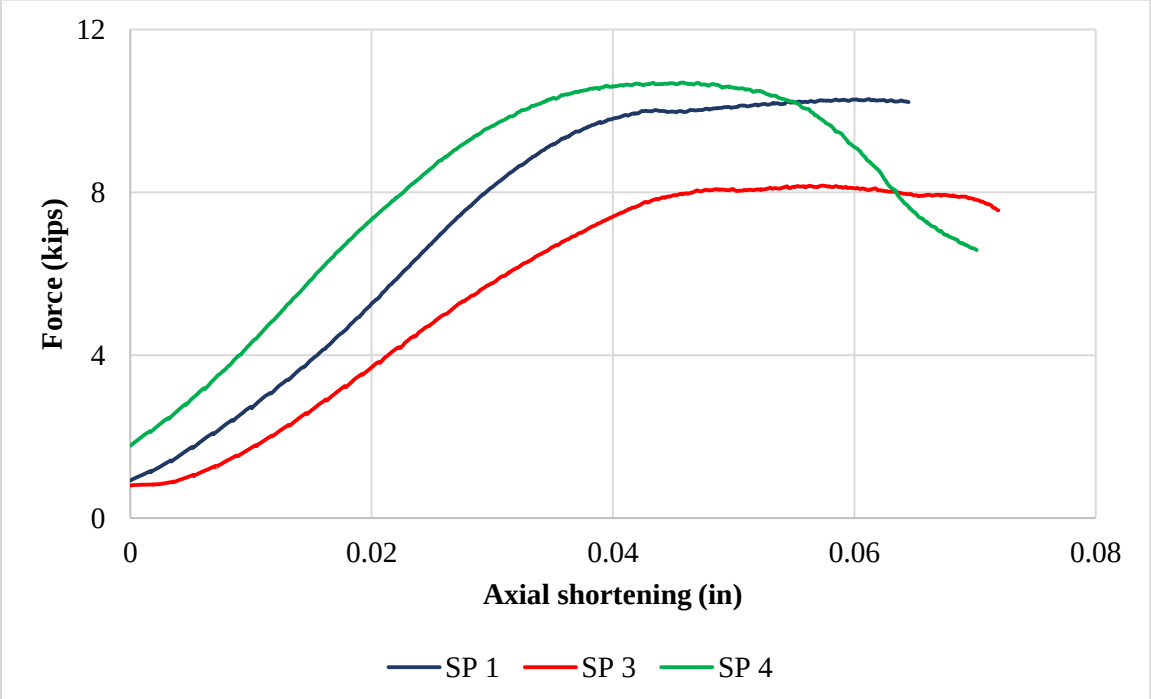

Figure 3. 7 Applied load-axial shortening curve obtained from 22ga HST testing

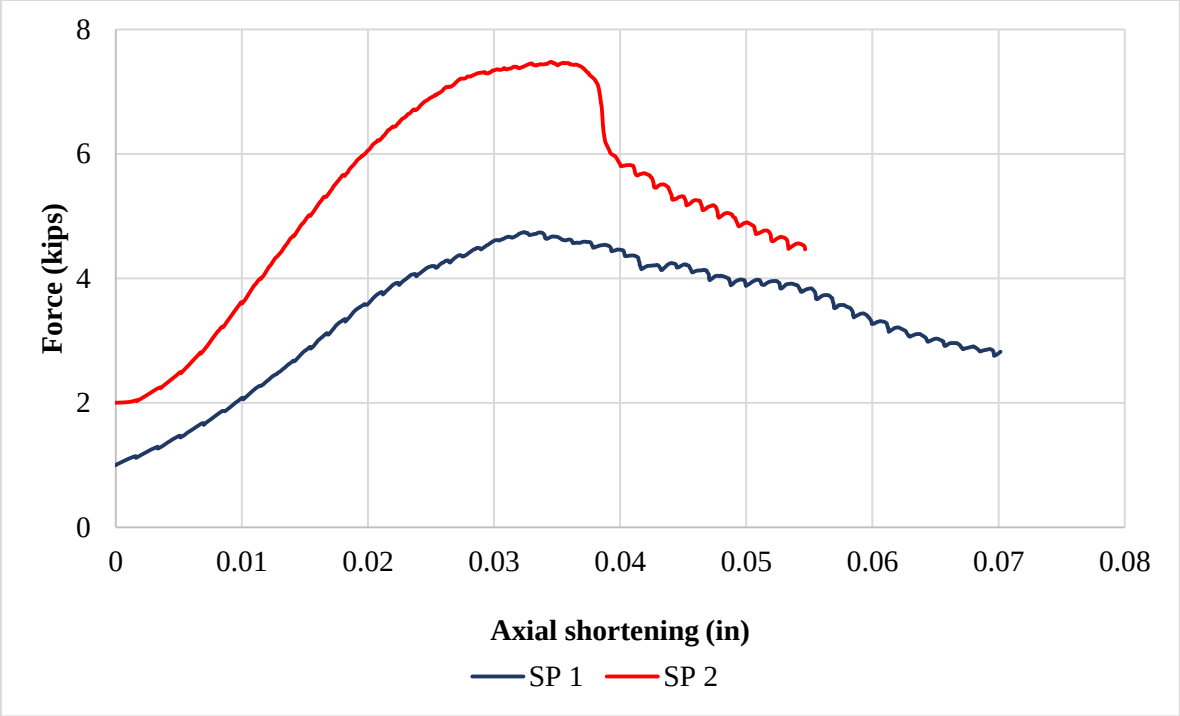

Figure 3. 8 Applied load- axial shortening curve obtained from 24ga HST testing

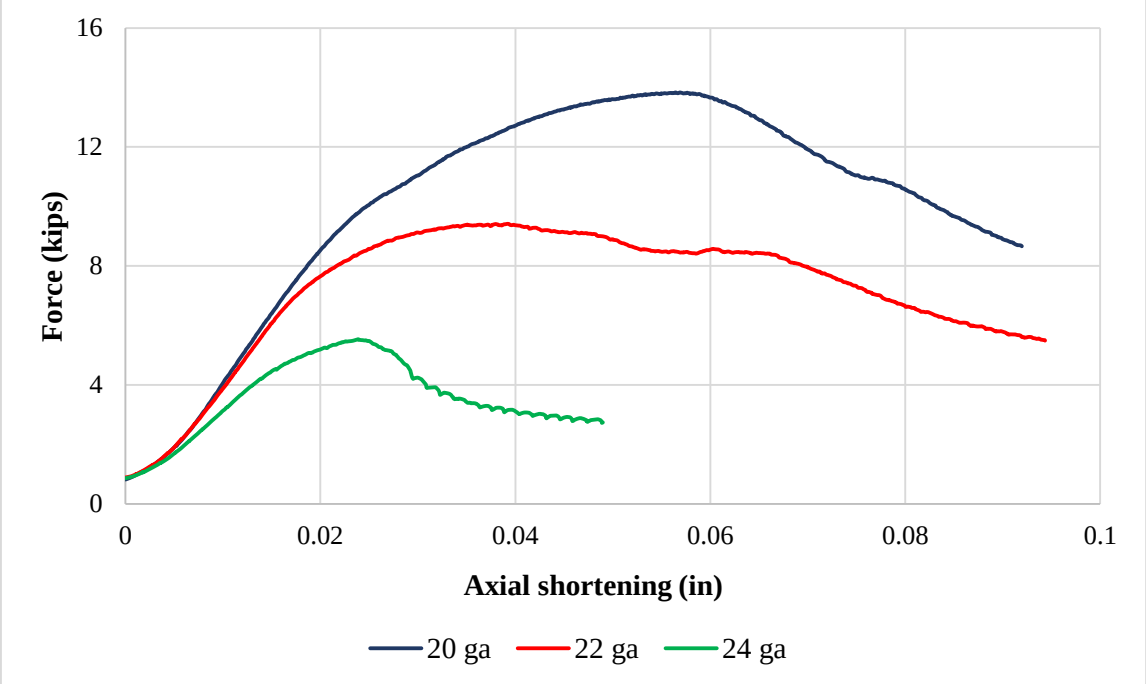

Figure 3. 9 Comparison of CCFT Type I specimens with varying thickness

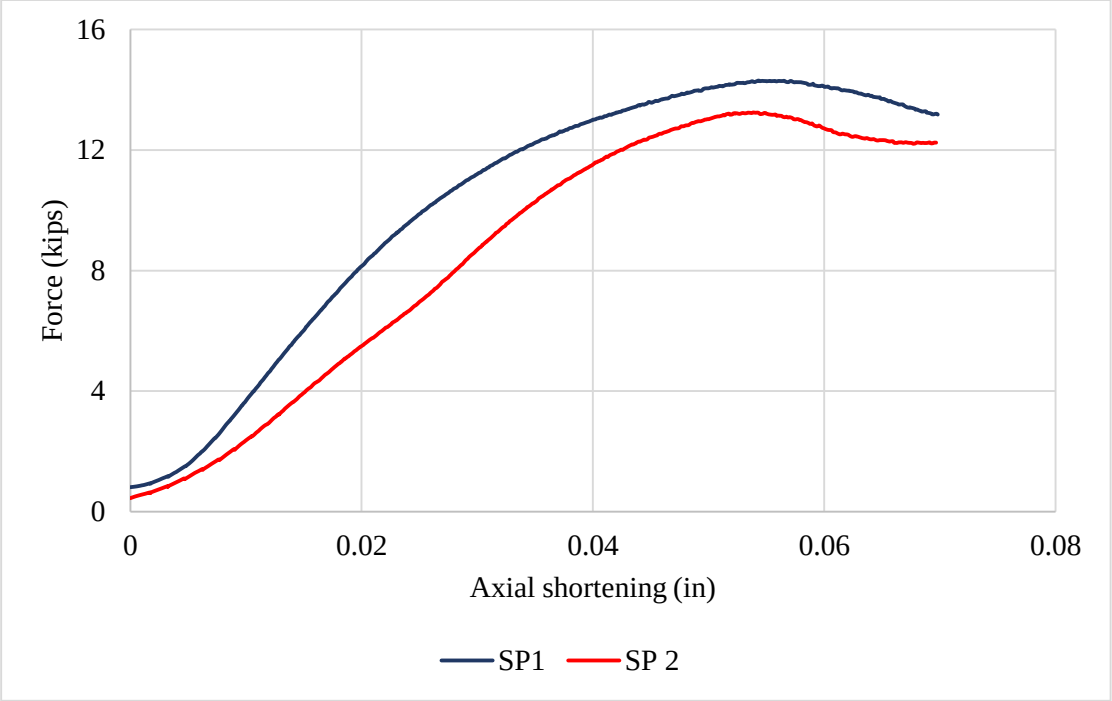

Figure 3. 10 Applied load-axial shortening curve obtained from 20ga CCFT Type II specimen testing

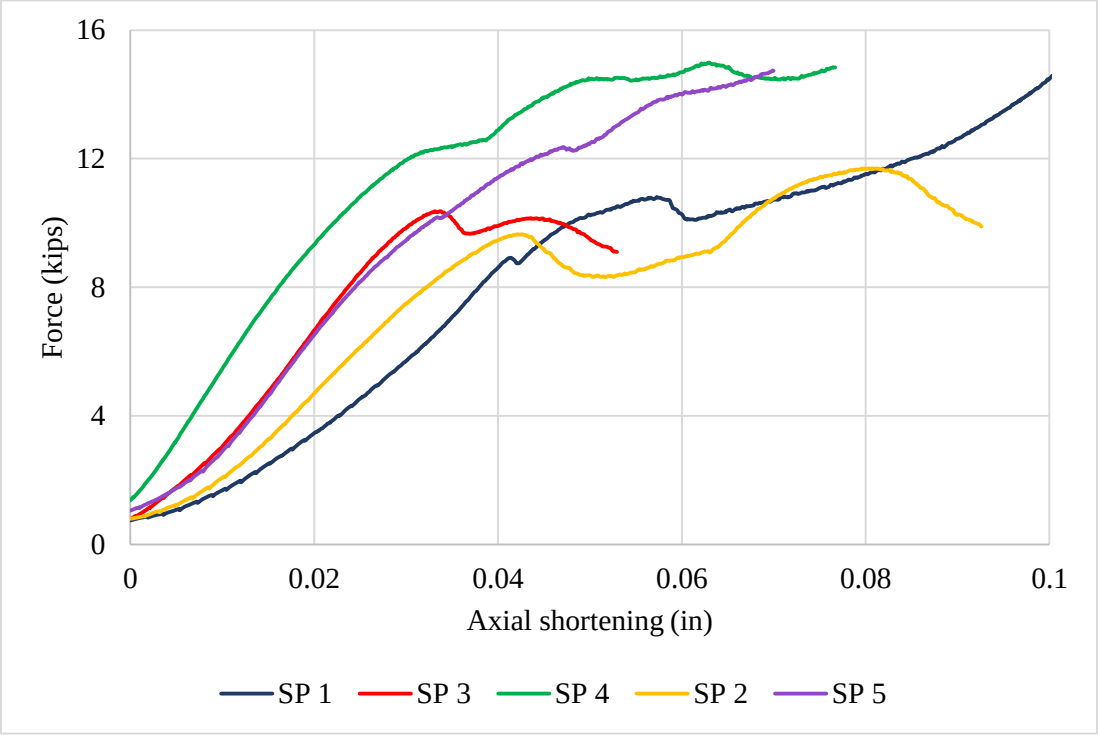

Figure 3. 11 Applied load- axial shortening curve obtained from 22ga CCFT Type II specimen testing

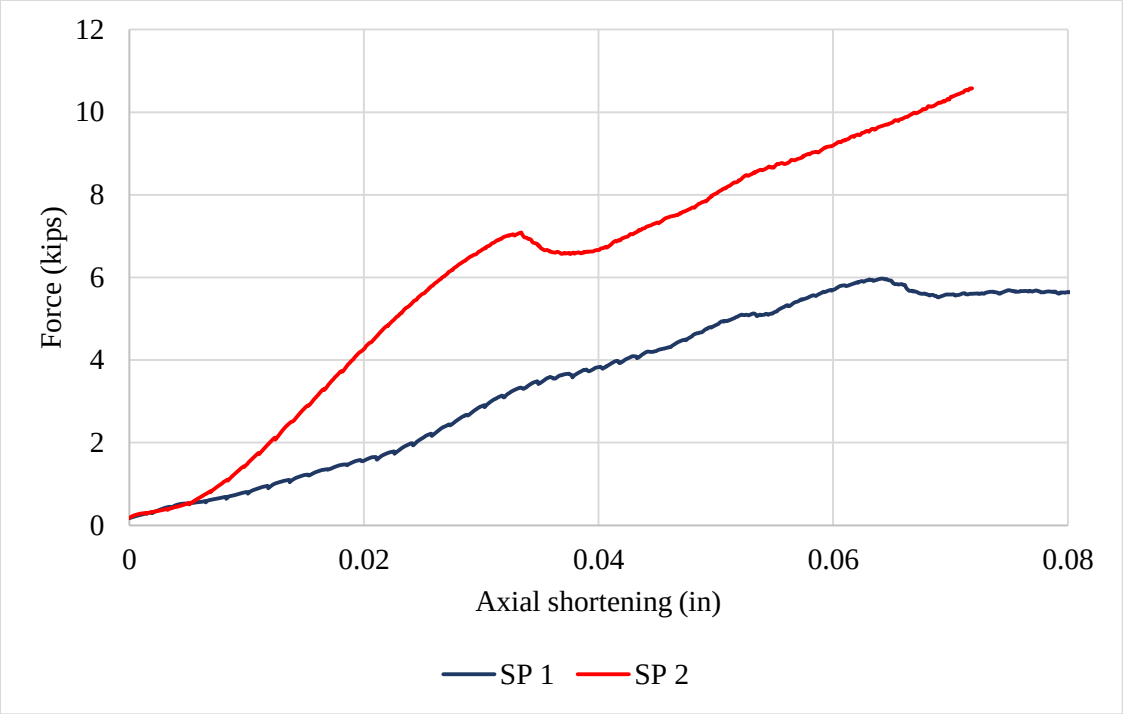

Figure 3. 12 Applied load-axial shortening curve obtained from 24ga CCFT Type II specimen testing

CHAPTER 4. ANALYTICAL PREDICTION

In general, a reliable analytical model needs to be develop so that meaningful comparisons can be made against the experimental results. In this work, the hollow steel tubes and the concrete filled tubes are modeled using ABAQUS (version 6.14-4), a finite element analysis software, in order to predict the local buckling load and the axial shortening of the tube. ABAQUS is a powerful tool for simulation, and it offers complete solutions for the analysis of concrete filled tubes with consideration to the steel tube, the concrete core, and the interaction between the two.

4.1 Parts and material properties

The dimensions of the steel tube and the concrete core are matched with the experimental specimen in order to compare the results. The steel tube and concrete are modeled using eight-node solid elements. All the tubes have an outside diameter of 5 inches, length of 16 inches and the thickness is varying depending on the gage thickness of the tube analyzed. The solid concrete core is similarly created with a diameter equal to inside diameter of the tube. The depth of the concrete core is reduced to apply load on steel tube alone. In order to define the meshing, the steel and concrete parts are partitioned. The concrete core is divided into equal size wedges (Figure 4.2). A datum plane is defined at an offset of 0.5 inch from the bottom surface of the steel tube and 0.5 inch from the top surface. This allows us to create the boundary condition similar to the experimental specimen where the top and bottom ends are fixed inside the slots provided in the platens.

The material properties of the steel and concrete are given in Appendix B.1 and B.2. For the steel material, the density of 0.246 lb/in^3 is used. The elastic property is defined using the Young's

modulus of the material. This obtained from the stress-strain curves obtained from coupon testing The Poisson's ratio for steel is taken to be equal to 0.3 based on many technical references. The plastic region in the stress-strain curve of the coupon test results starting from the yield stress defines the plastic property of the material with plastic strain value starting from zero. The strain hardening plastic property for steel is taken from a Ramberg-Osgood curve matching the coupon test results, shown in Figure B .1.3.

The elastic properties for concrete material is defined in a similarly to steel. A density of 0.0868 lb/in^3 is considered. The Young's modulus is calculated using the approximate equation Eq 19.2.2.1.b provided in ACI 318-14 which requires the compressive strength of concrete. This is obtained from the compression testing of the concrete cylinders. And a poisons ratio of 0.2 is used for concrete.

The plastic material properties are defined using Concrete Damage Plasticity model which is available in ABAQUS material library. Dilation angle controls the amount of plastic volumetric strain developed during plastic shearing and assumed constant during plastic yielding and is considered to be 36°. The eccentricity *e* is determined using Eq. 4.1 and Eq. 4.2 (Bazant & Jirásek, 2002)

$$\varepsilon = \frac{f_t}{f_{bc}} \frac{(f_{bc}^2 - f_c^2)}{(f_c^2 - f_t^2)} \quad \text{(Eq. 4.1)}$$

$$e = \frac{(1 + \varepsilon)}{(2 - \varepsilon)} \quad \text{(Eq. 4.2)}$$

In these equations, f_{bc} is the equibiaxial compression equal to 1.16 f_c (Kupfer et al, 1969). The parameter f_{b0}/f_{c0} is the ratio of biaxial strength to uniaxial strength also called the compressive stress ratio (Lee and Fenves, 1998) is determined using Eq. 4.3.

$$\frac{f_{bo}}{f_{c0}} = \frac{(\alpha - 1)}{(2\alpha - 1)} \qquad \text{(Eq. 4.3)}$$

Where parameter α is considered to be equal to 0.15. The value of space *K* is considered to be 0.67 (Chen and Han, 2007) and the viscosity parameter is taken as zero, which is the default value assumed in ABAQUS. The compressive yield stress f_c is equal to the concrete compressive strength and the inelastic strain equals zero. The tensile yield stress f_t for uncracked concrete is calculated using the empirical formula provided by Table 24.5.2.1 in ACI 318-14 which uses the value of compressive strength of concrete. The cracking strain equals to zero. The materials hence defined are attached to the parts define in the ABAQUS meshing.

4.2 Finite element meshing

A solid type of elements was created in order to clearly define the boundaries of the elements and their interfaces. The partitions created will allow seeding on the edges of the partition, which helps in defining the type of meshing desired. Seeding is done based on the determined meshing type and size, which gives more accurate results in less computational time. The concrete core has a wedge type meshing, while a fine hex mesh with a sweep technique is used to mesh the other parts. Figure 4.2 shows the meshing of a steel tube, and Figure 4.3 shows the finite element meshing of the infill concrete.

4.3 Boundary conditions and loading

The boundary conditions are simulated according to the experimental conditions which considers the restraint due to platens. Using the defined datum plane, additional restraints are provided in order to simulate the tube inside the platen. Two reference points RP1 and RP2 are defined along the centerline of the axis at the bottom and top, respectively. These reference points are coupled to the bottom and top steel surfaces, enabling an easy way to define the load and constraints. The bottom surface of the steel tube is fixed in all degrees of freedom. The top surface of the steel tube is restrained in all degrees of freedom except in the vertical displacement (U3) in the direction of the application of the load (global Z). The steel tube is restrained at the datum reference plane in all degrees of freedom except the displacement in the direction of loading (U3).

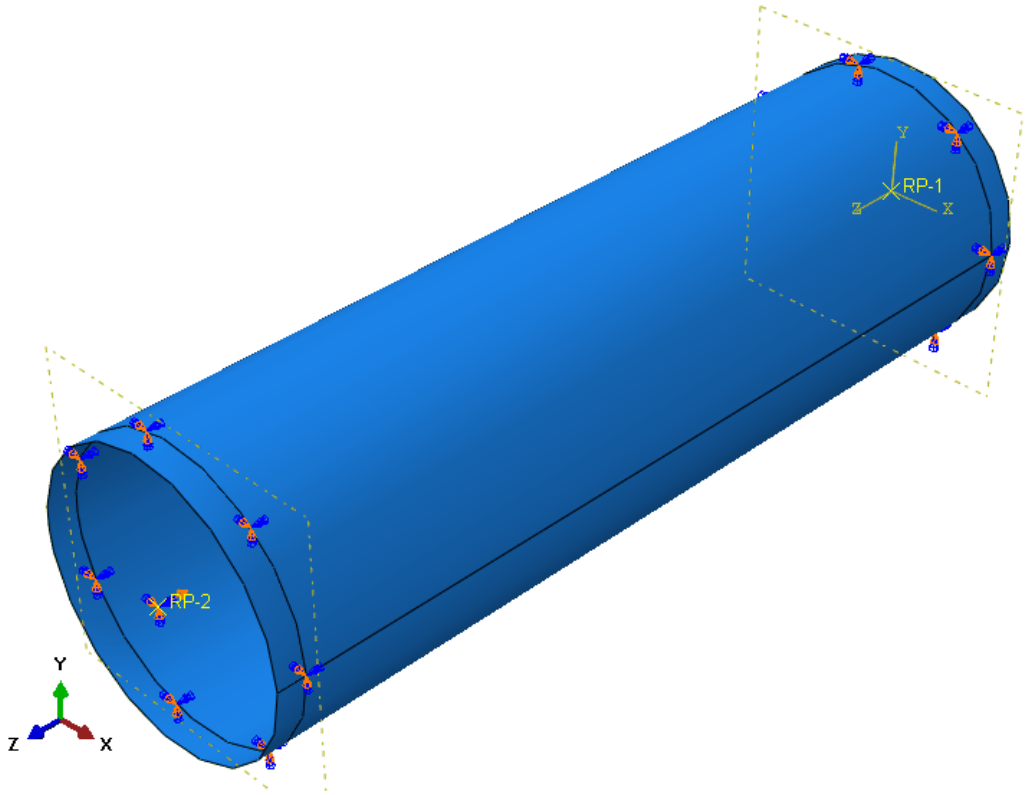

Figure 4. 1 Boundary conditions defined in the ABAQUS model

The static load is then applied in increments to the reference point (RP2) at the top of the steel tube, restraining the axial displacement of reference point RP1 in the direction of loading (U3).

4.4 Steel to concrete interaction

The concrete core does not have any boundary conditions specified. The interface between the concrete and the steel is defined only by a surface friction (constraint in tangential direction) of 0.5 applied to the outer surface of the concrete and inner surface of the steel tube. The friction between these surfaces remains as long as they are in contact. Once the bond between the steel and concrete is lost, the friction no longer contributes to the capacity of the CFT. There are no additional bonds (mechanical or chemical) between the concrete infill and steel tube. In order to avoid penetration of concrete and steel into one another, hard contact (constraint in normal direction) is defined at the interface. A reference point is created at the center of the top surface, which is constrained to the top surface of the steel (Figure 4.3). The static load is applied through this reference point as a concentrated load.

4.5 Analysis and results

The model is analyzed for static loading and the buckling load is determined. The applied load-axial shortening plots are obtained in order to compare them with the experimental results. The plots are obtained by applying incremental concentrated loads on the member and obtaining the maximum displacement for each load applied. The applied load- axial shortening curve for a Hollow Steel Tube (HST) is shown in Figure 4.6 while a CCFT of Type I for the three tube thicknesses considered for the experiment is shown in Figure 4.7. The local buckling load is very clear on the plots where there is a sudden change in the slope of the curve. The deformed shape of

the CCFT Type I (20ga) specimen is shown in Figure 4.5, where the buckling wavelengths of the tube can be clearly seen.

The initial stiffness (slope) of the member determined from the load-axial deformation plots is comparable to the stiffness calculated theoretically (EA/L). However, the elastic response obtained from the finite element model does not match the experimental values. In order to get more accurate results, dynamic explicit model should be used which allows displacement loading.

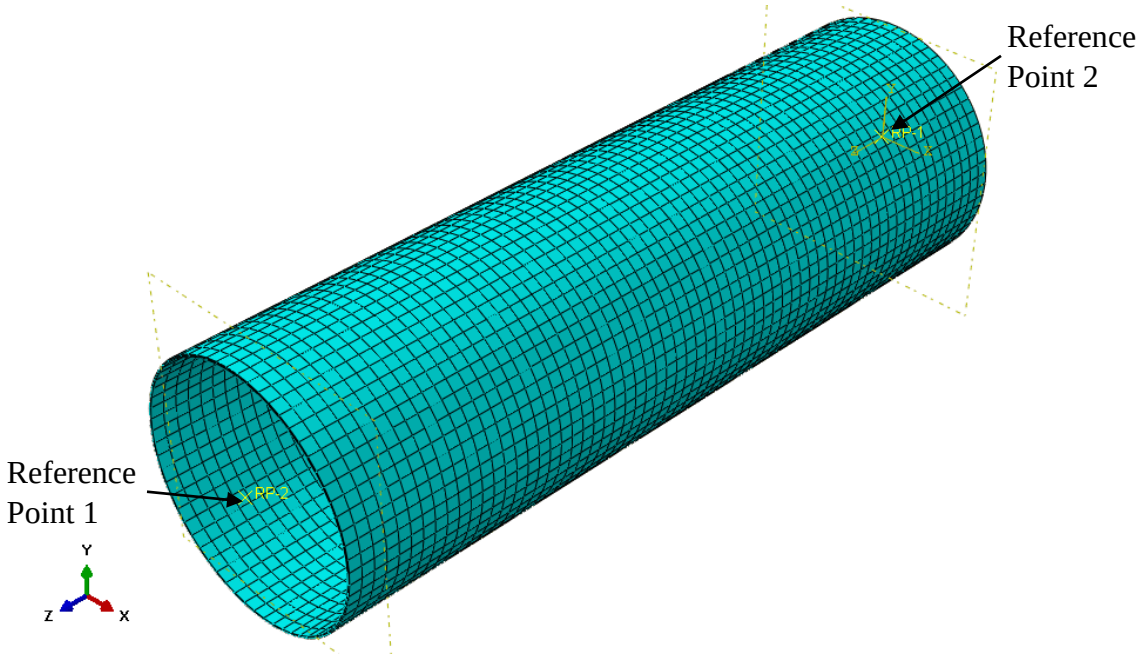

Figure 4. 2 Steel tube meshing

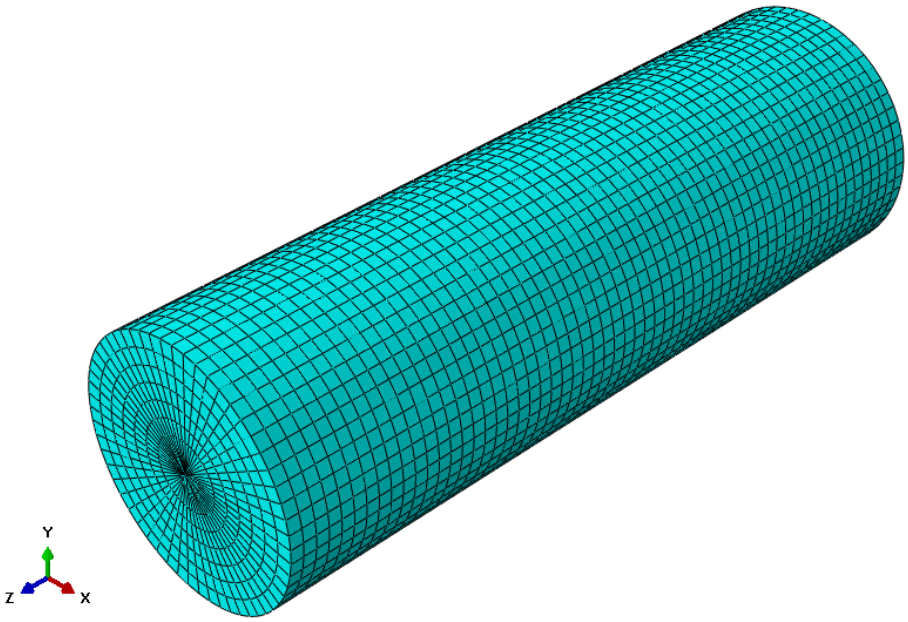

Figure 4. 3 Infill concrete meshing

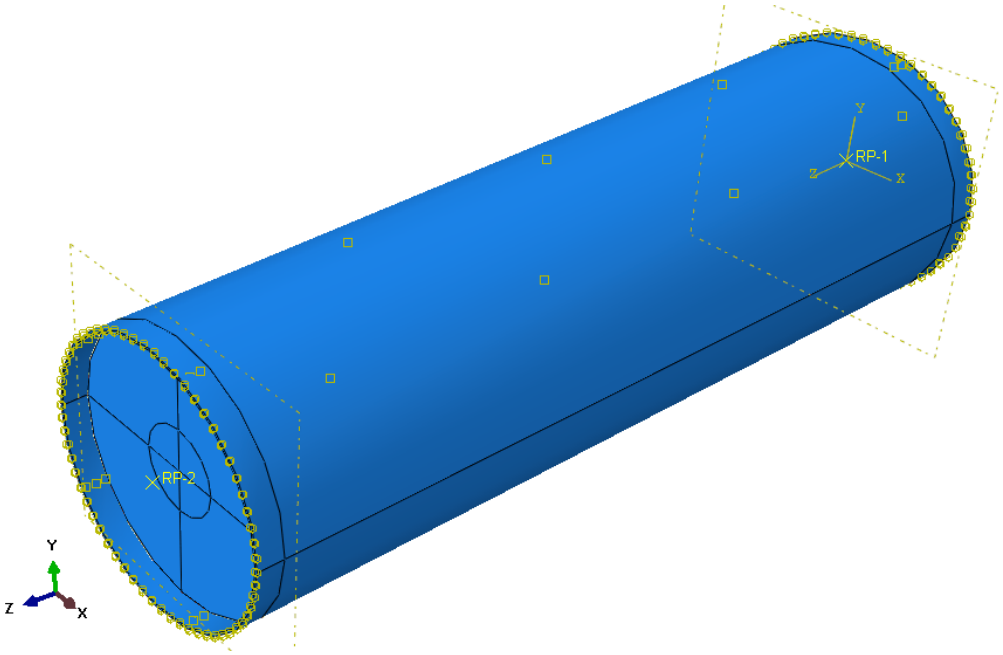

Figure 4. 4 CFT assembly with constraints

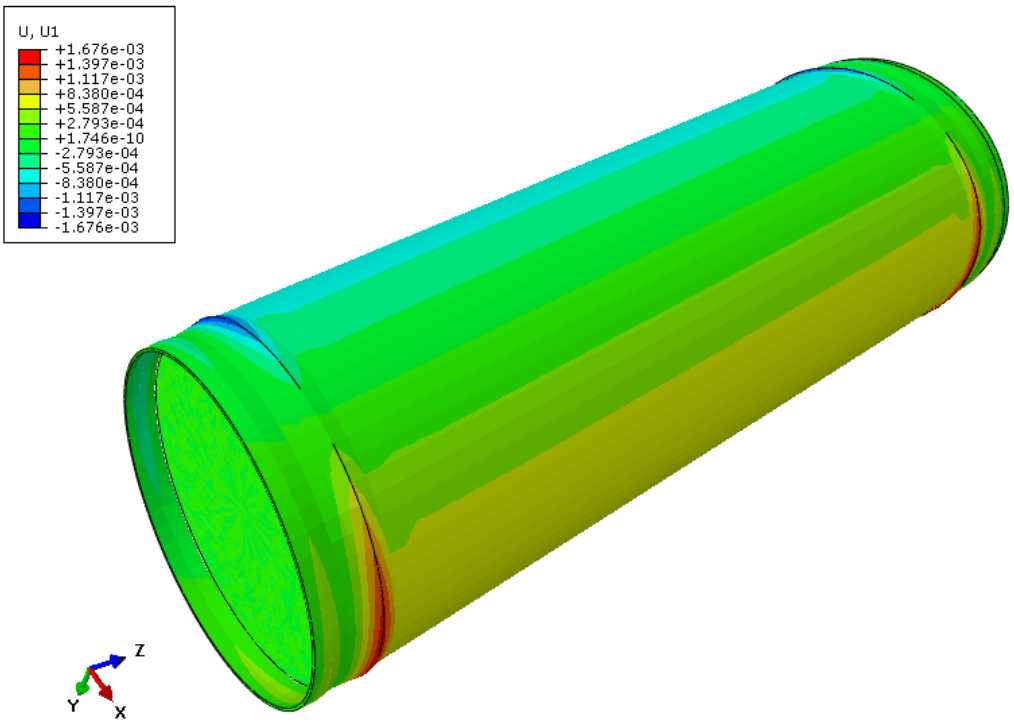

Figure 4. 5 Deformed shape of CCFT with 20 ga steel tube

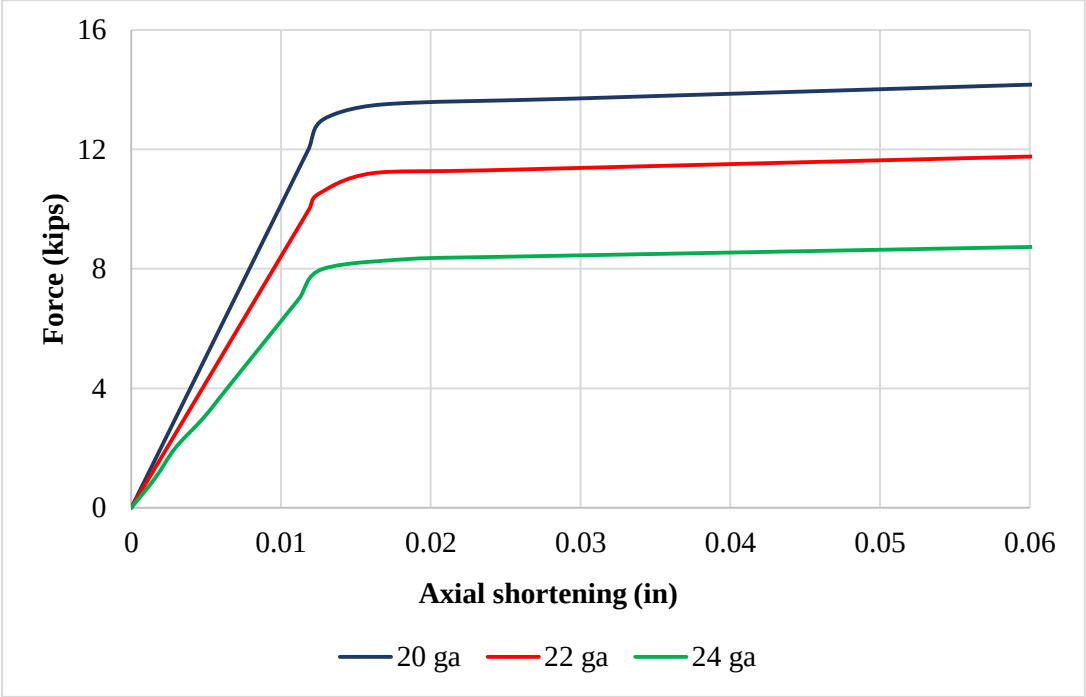

Figure 4. 6 Comparison of applied load- axial shortening curve for HST specimens

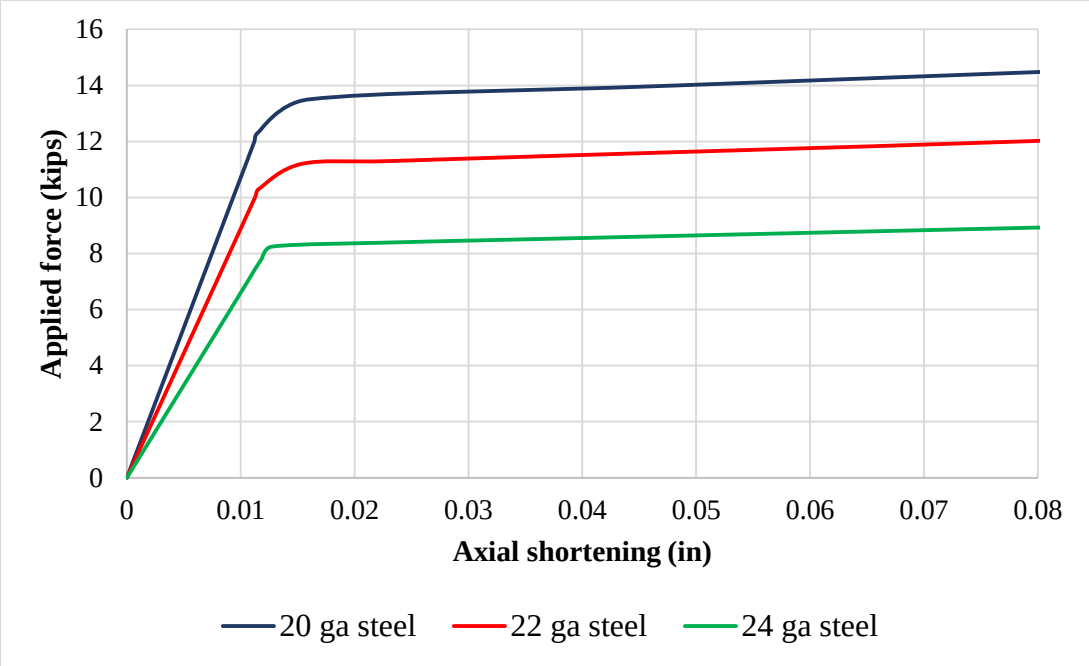

Figure 4. 7 Comparison of applied load- axial shortening curve for Type I CCFT specimens

CHAPTER 5. THEORITICAL PREDICTION

The theoretical prediction of buckling loads and wavelengths are based upon the work by Zhang (2009) which developed closed form solutions for hollow and filled tubes. This theory calculates the ultimate failure loads of CCFTs, where the load is applied on both steel and concrete surfaces. The typical failure of CCFT columns includes buckling of the steel tube and crushing of the infill concrete. The ultimate strength is determined by considering the one-way buckling mode of the steel tube with concrete infill. The ultimate buckling load, or failure load, is given by Eq. 5.1.

$$N_T = \sigma_{cr} A_s + f_c' A_c \qquad \text{(Eq. 5.1)}$$

$$\sigma_{cr} = \frac{5}{3}\frac{t}{R}\sqrt{\frac{(B'D' - C'^2)}{3}} \qquad \text{(Eq. 5.2)}$$

The theoretical buckling load for the CCFT has two contributing components. The first part of N_T is the buckling load of the steel tube, $Ns = \sigma_{cr}A_s$, in which σ_{cr} is the critical buckling stress of the steel tube and A_s is the area of the cylinder. The value of σ_{cr} is constrained by the concrete infill and is given by Eq. 5.2. The second part of N_T is the crushing strength of the concrete, or $N_C = f'_cA_c$, where f'_c is the compressive strength of the infill concrete, and A_c is the area of the concrete section. The concrete encased in steel has better development of strength due to the protection against the environment and against the spalling of concrete, which eliminates the use of the usual performance factor of 0.85. Thus, the effects of concrete confinement on steel shells and steel tube confinement of concrete are considered. The concrete core has a very high modulus of elasticity, and hence can be considered rigid.

To determine the critical stress in the steel tube, the parameters considered are the radius *R*, which is measured to the center line of the tube, and the thickness *t* of the tube. The thickness varies for the three different gages of material considered in this experimental work. One can note that Eq. 5.2 is very sensitive to material properties. The tangent modulus of elasticity E_t is determined from the well-established formula put forth by Ramberg and Osgood (1943) (Eq. 2.15). An idealized stress-strain (Figure B.1.4) curve is considered, which is based on the actual coupon test results. Since the material is not purely elastic, idealizing them as purely elastic will give very conservative critical stress values for elastic buckling. For more realistic predictions, plastic buckling is considered. The bifurcation stresses predicted by the J_2 incremental theory are always higher compared to the deformation theory results (Zhang, 2010).

The theoretical critical buckling load N_T for hollow tubes is summarized in Table 5.1.

Table 5. 1 Summary of buckling load for hollow tubes

Specimen gage	Thickness t (in)	D/t	σ_{cr} (ksi)	A_s (in^2)	N_T (kips)
20	0.0392	128	24.62	0.61	15.0
22	0.0325	154	20.41	0.51	10.4
24	0.0241	207	15.13	0.38	5.7

Since the buckling load N_T for CCFT considers the compressive strength of the concrete, it gives a very high value. It can be seen in Table 5.2.

Table 5. 2 Summary of buckling load for concrete filled tube

Specimen gage	Thickness t (in)	D/t	σ_{cr} (ksi)	A_s (in^2)	f'_c (ksi)	A_c (in^2)	N_T (kips)
20	0.0392	128	41.03	0.61	7	19.02	158.2
22	0.0325	154	34.01	0.51	7	19.13	151.1
24	0.0241	207	25.22	0.38	7	19.26	144.3

CHAPTER 6. COMPARISON OF THE RESULTS

A set of experiments on short tube sections with hollow core and concrete filled core were performed in the laboratory in order to understand local buckling behavior of CFTs and to check the feasibility of performing such experiments for the future work. A finite element analysis was performed for the specimens used for the experiments in order to verify the results. In addition, the buckling load obtained from the experiment was verified using a theoretical approach. The results obtained from these experimental, analytical and theoretical approaches are compared in this section.

6.1 Hollow Steel Tubes (HST)

A set of experiments are performed on hollow tubes to understand the effect of the core. From the experiments, a plot of applied load (kips) versus axial shortening of the tube (in) was obtained. This was compared to the applied load- axial shortening obtained from the finite element analysis (Chapter 4). Typical results are presented in Figures 6.1 through 6.3. The buckling load obtained from the theoretical approach (Chapter 5) is shown as a horizontal line in the figures. This buckling load is just representative to provide a comparison with the experimental and analytical work. The FEA results for the hollow tubes show reasonable correlation with the lab results given that end effects, initial imperfections, residual stresses, and seam effects are not considered in the analyses.

6.2 Concrete Filled Tubes (CFT)

6.2.1 Concrete Filled Tubes Type I

The first set of concrete filled tubes were casted with an inch gap (hollow core) at the ends. This was done in order to apply the load only on the steel tube since the study is on local buckling of the steel tube. The applied load- axial shortening plot obtained from the experiment is compared with the finite element model results (Figure 6.4, 6.5 and 6.6). The buckling loads predicted through the finite element analyses are slightly higher than the experimental results, but they can be considered to be in good agreement. Since only one experiment was run on each type I CFT member, the results cannot be ascribed any statistical significance. The buckling mode of CCFT Type I with 22 ga steel is shown in Figure 6.12 and it can be compared to the buckling mode obtained from the finite element analysis which is shown in Figure 6.13.

6.2.2 Concrete Filled Tubes Type II

The type I CFT members exhibited similar buckling modes to that of hollow steel tubes. In order to obtain a buckling mode more consistent with the one expected for an specimen with a rigid core, type II CFT specimens were cast with an infill gap (hollow core) of about 0.1 inches deep at the ends. This minimal gap in the core at the ends intended to ensure that loading would be on the steel tube alone (see Figure B.2.1 and B.2.2). The results obtained from the finite element analysis are compared with the experimental results in Figures 6.7 through 6.9. The buckling load obtained experimentally for this case is comparable to the analytical from the finite element model. The data in Figure 6.9 is hard to discern but local buckling appears to have occurred when a slight dip in the curve occurred; rapid reloading followed perhaps because the gap closed rapidly for these

specimens. The buckling mode of the 20ga hollow tube is shown in Figure 6.10 and it can be compared to the buckling mode obtained from the finite element analysis presented in Figure 6.11.

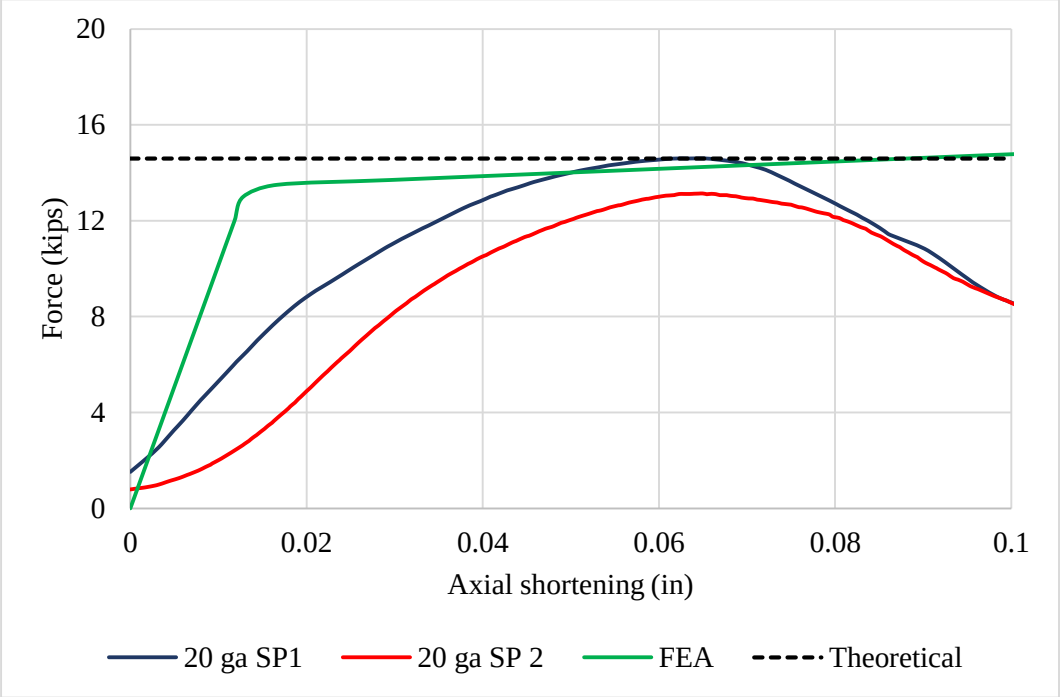

Figure 6. 1 Comparison of buckling loads for 20ga hollow tube

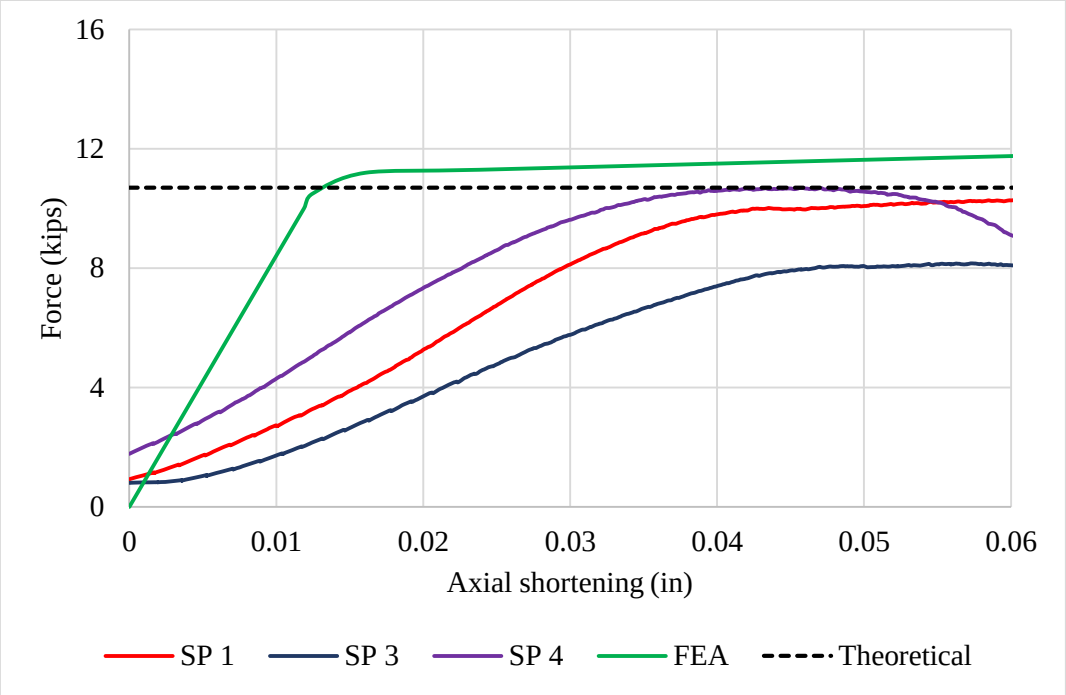

Figure 6. 2 Comparison of buckling loads for 22ga hollow tube

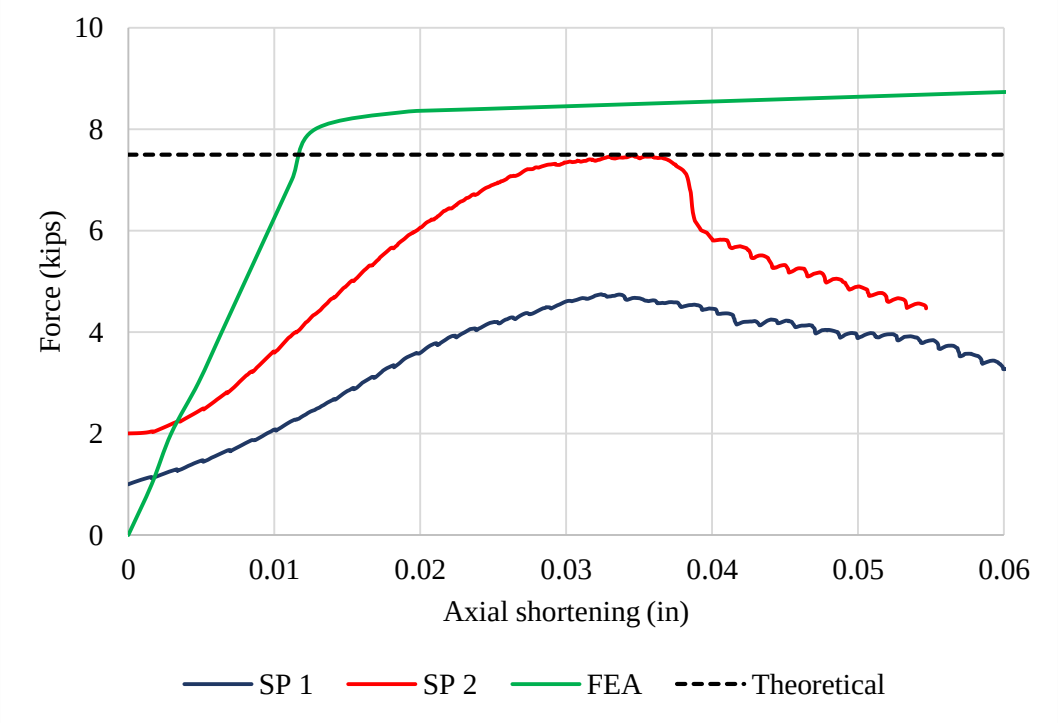

Figure 6. 3 Comparison of buckling loads for 24ga hollow tube

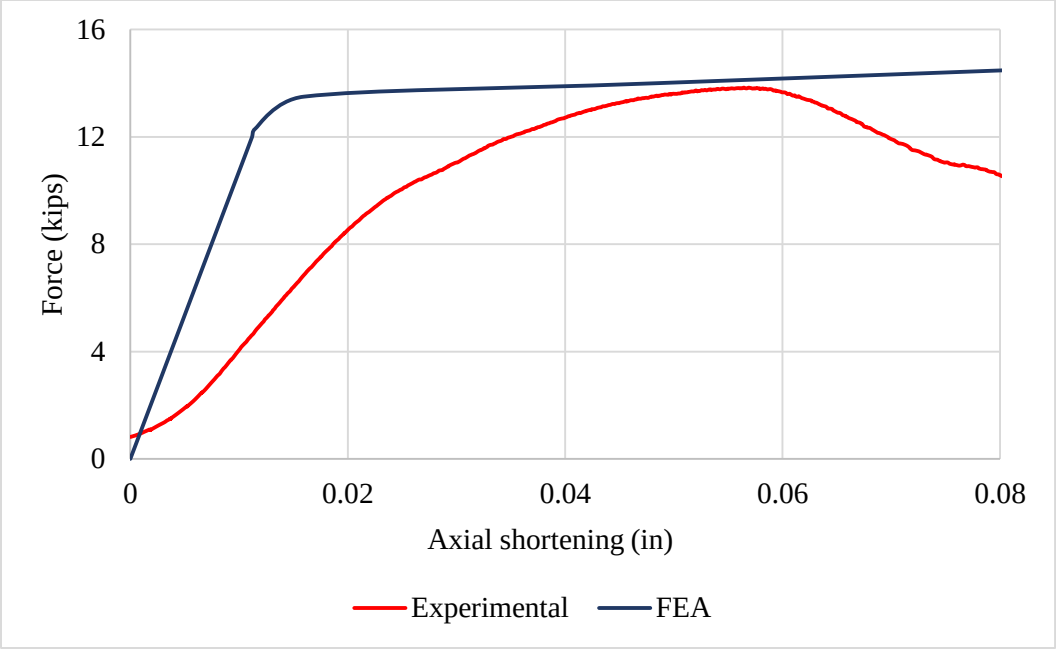

Figure 6. 4 Comparison of buckling loads for 20ga CCFT Type I specimen

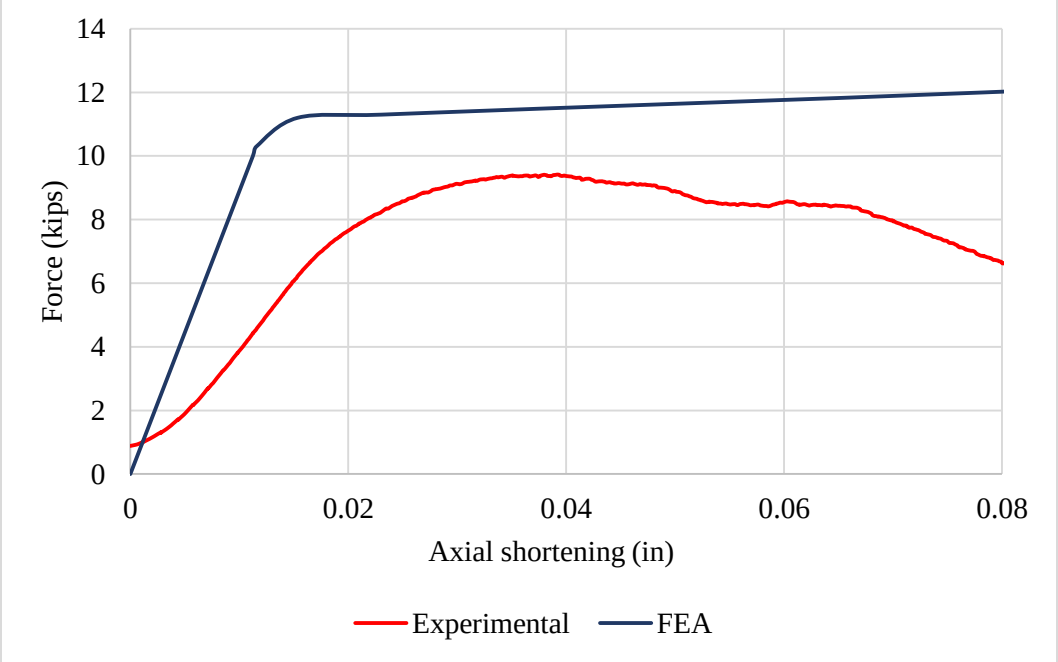

Figure 6. 5 Comparison of buckling loads for 22ga CCFT Type I specimen

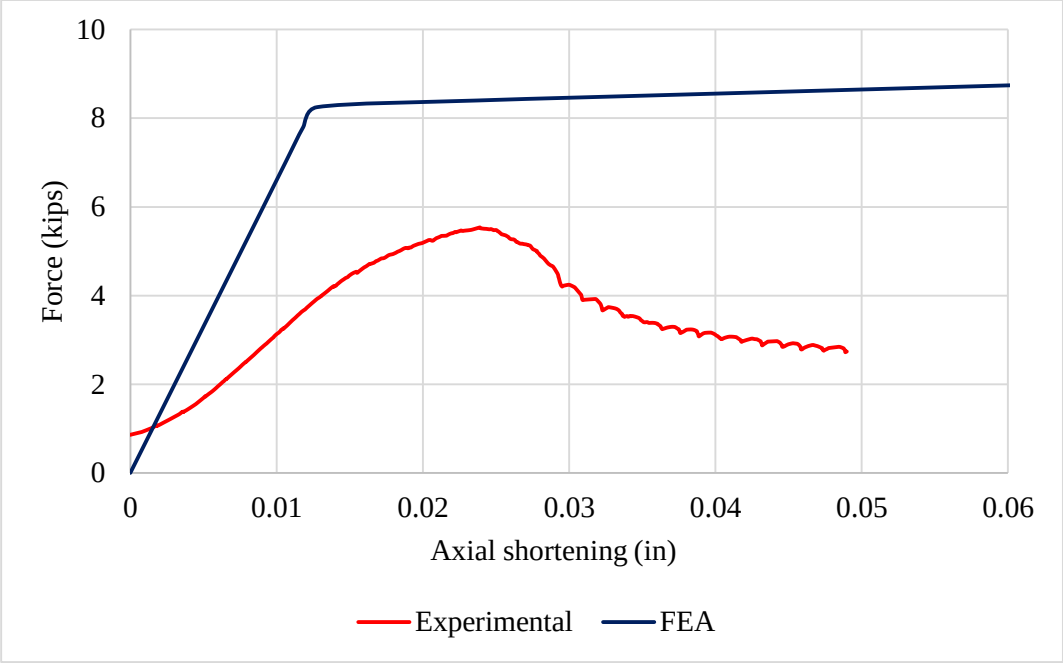

Figure 6. 6 Comparison of buckling loads for 24ga CCFT Type I specimen

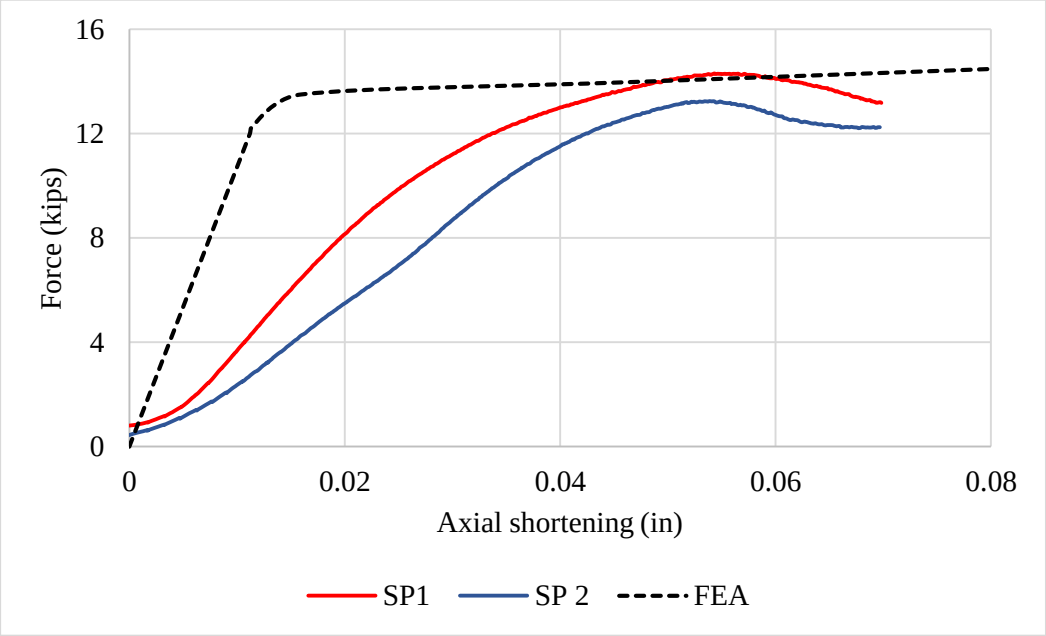

Figure 6. 7 Comparison of buckling loads for 20ga CCFT Type II specimen

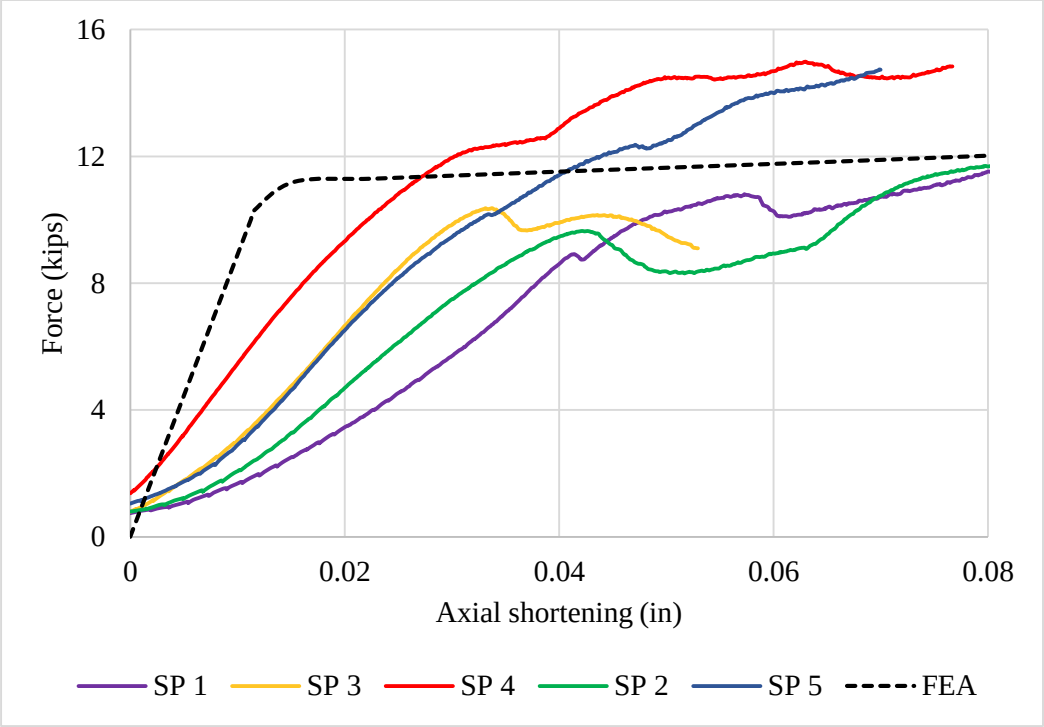

Figure 6. 8 Comparison of buckling loads for 22ga CCFT Type II specimen

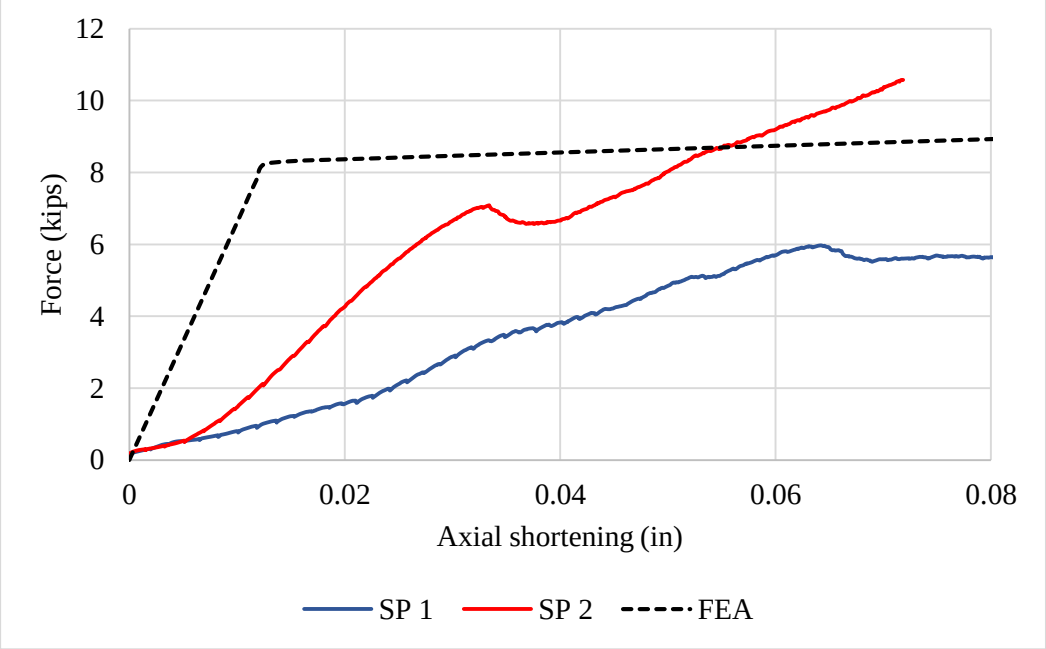

Figure 6. 9 Comparison of buckling loads for 24ga CCFT Type II specimen

Figure 6. 10 Buckling shape of 22-HST-01 obtained from laboratory experiment

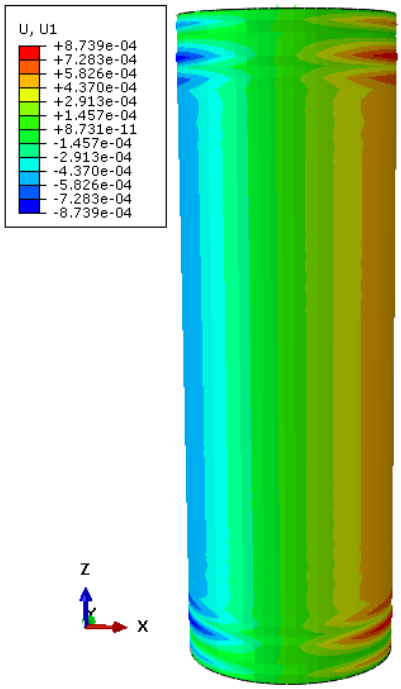

Figure 6. 11 Buckling shape of 20-HST-01 obtained from ABAQUS model

Figure 6. 12 Buckling shape of 20-CFT-I-01 obtained from laboratory experiment

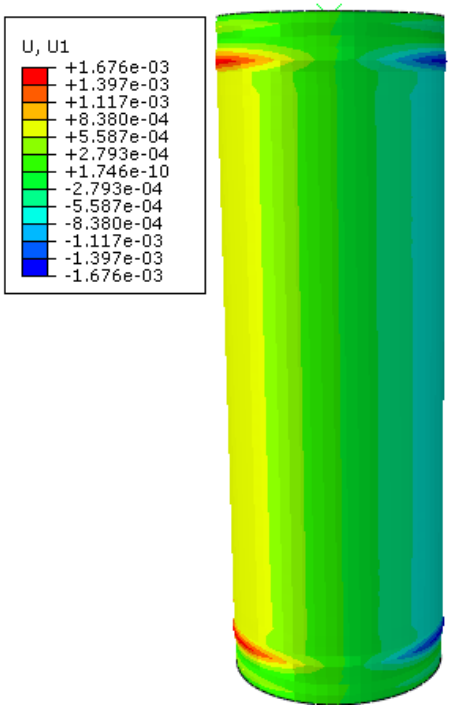

Figure 6. 13 Buckling shape of 20-CFT-I-01 obtained from ABAQUS model

CHAPTER 7. SUMMARY AND CONCLUSIONS

This thesis presents the development and validation of a testing methodology and the resulting load-axial shortening curves for both hollow steel tubes and two types of circular concrete filled tubes. The ultimate end of the work was to determine if this testing methodology could be used to perform a future large experimental parametric study on tubes with high strength steels and slender wall sections. In addition, the work developed and validated a finite element model that could be used for further parametric studies. The steel tubes had a high diameter to thickness ratio, ranging from 127 to 207.

The results obtained from the experimental work, analytical models and theoretical predictions are compared in Chapter 6. Some of the major conclusions from this work are:

- The experiments were performed on short specimens (L/D ratio of 3) to observe the local buckling mode of failure and to determine the critical buckling load associated with this mode of failure. The buckling loads obtained from the experiments involve considerable uncertainties due to lack of measurement of initial imperfections and residual stresses. The additional imperfections in the specimens from the spot welding, non-uniform ends, initial out of plumbness of the specimen, assumed material model, and lack of perfect control for the degrees of freedom which are detailed in section 3.5.3. All efforts were made to minimize these errors and obtain the local buckling of the tube as accurately as possible with the available facilities.
- The raw data from the tests are presented without any modification; because of the large number of uncertainties previously described, the results obtained are not consistent with the expected values.

- The short specimens can be used effectively to perform tests on local buckling. The tubes can be fabricated as presented in this work but the imperfections due to fabrication and spot welding need to be carefully considered in the analytical models in order to obtain more accurate results.
- The local buckling load predicted using the FE approach gives a slightly higher value compared to the value obtained from the experimental work. Considering the uncertainties involved in the experiments stated above, the experimental values can be considered to be valid.
- The critical buckling load obtained from the experiments were also compared with the theoretical approach. The plastic buckling load is computed for both hollow tube and concrete filled tube using the J_2 deformation theory presented in Chapter 5. The bifurcation load obtained is in good agreement with the experimental results of the hollow tube but slightly on the higher side. The imperfections in the experiment caused these discrepancies. However, this approach cannot be used to validate the CCFT experimental results since the theory assumes complete infill of concrete.
- It should be observed that the load transfer to the concrete surface plays a very important role in contributing to compressive strength of the columns. Even the slightest of the gap can cause the steel tube to fail early due to local buckling.

CHAPTER 8. FUTURE WORK

The present study is focused on the feasibility study of testing the short specimens with higher section slenderness for local buckling. From the experimental observation the following points are suggested in order to obtain more accurate results.

- The geometric imperfections to be reduced to minimum.
- The end restraints should be carefully designed. The outside diameter of the specimen should maintained and a snug fit into the platen slots to be ensured. Careful attention should be paid during concrete casting since the thin steel tube has a tendency to deform when the wet concrete is poured into it and compacted.
- The unavoidable imperfections need to be considered in the finite element analysis results and should be modified to obtain accurate results.
- The experimental method appears to be valid, with further refinements, to carry out further parametric studies on the effect of high strength steel and concrete on tubes with slender walls.

APPENDIX A. EXPERIMENTAL DATABASE

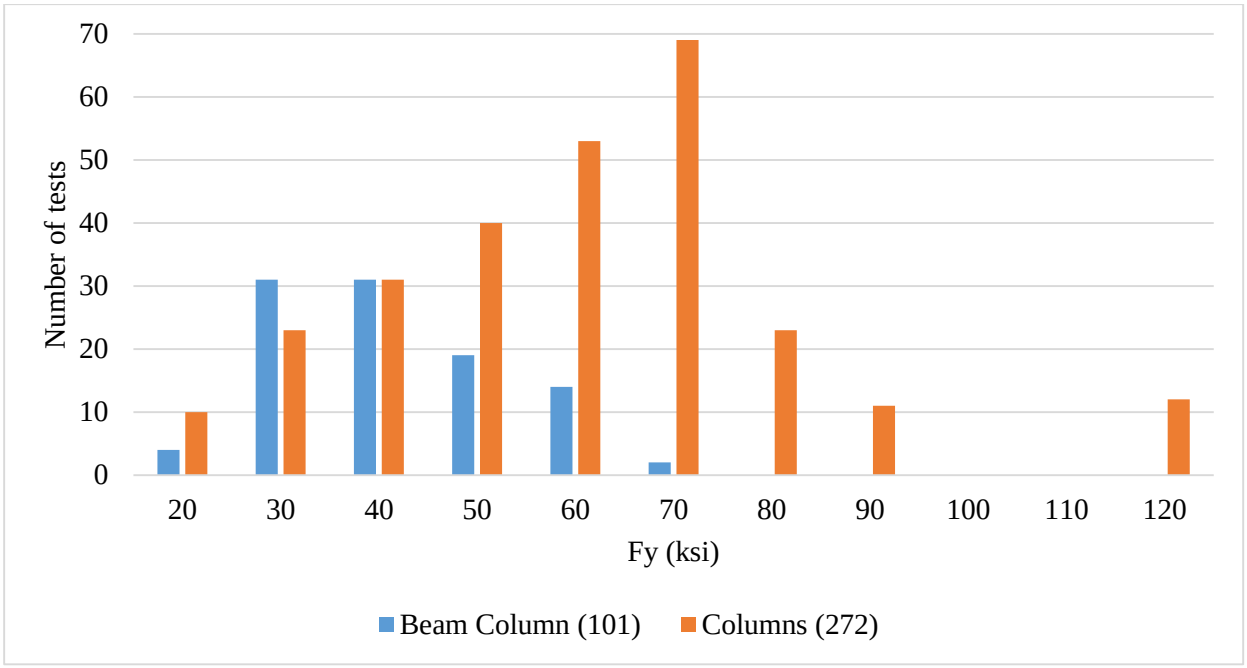

Figure A.1 Frequency distribution of F_y for CCFT column database of all tests

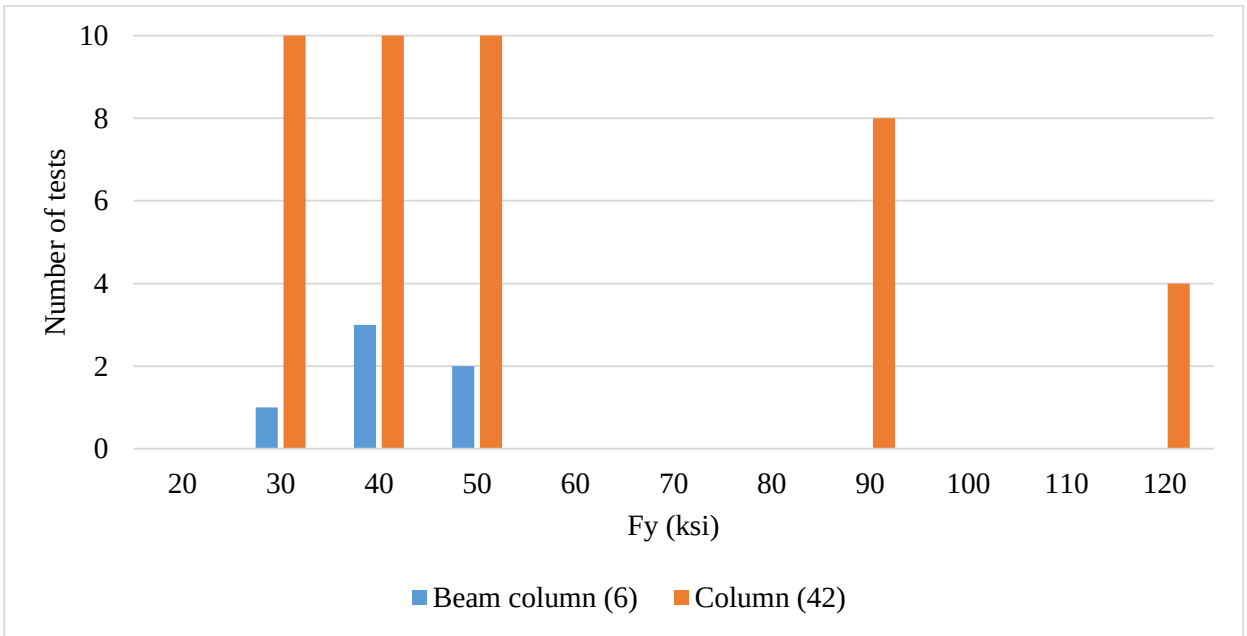

Figure A.2 Frequency distribution of F_y for CCFT column database failing in local buckling

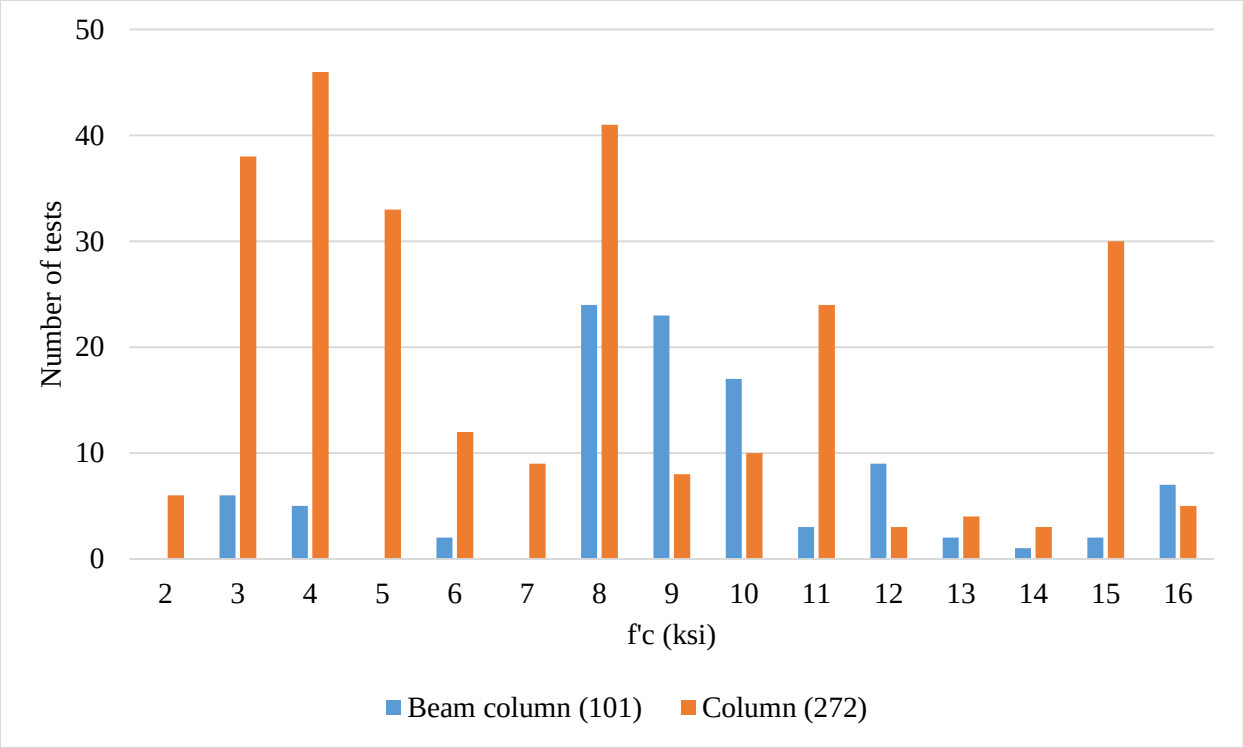

Figure A.3 Frequency distribution of f'_c for CCFT column database of all tests

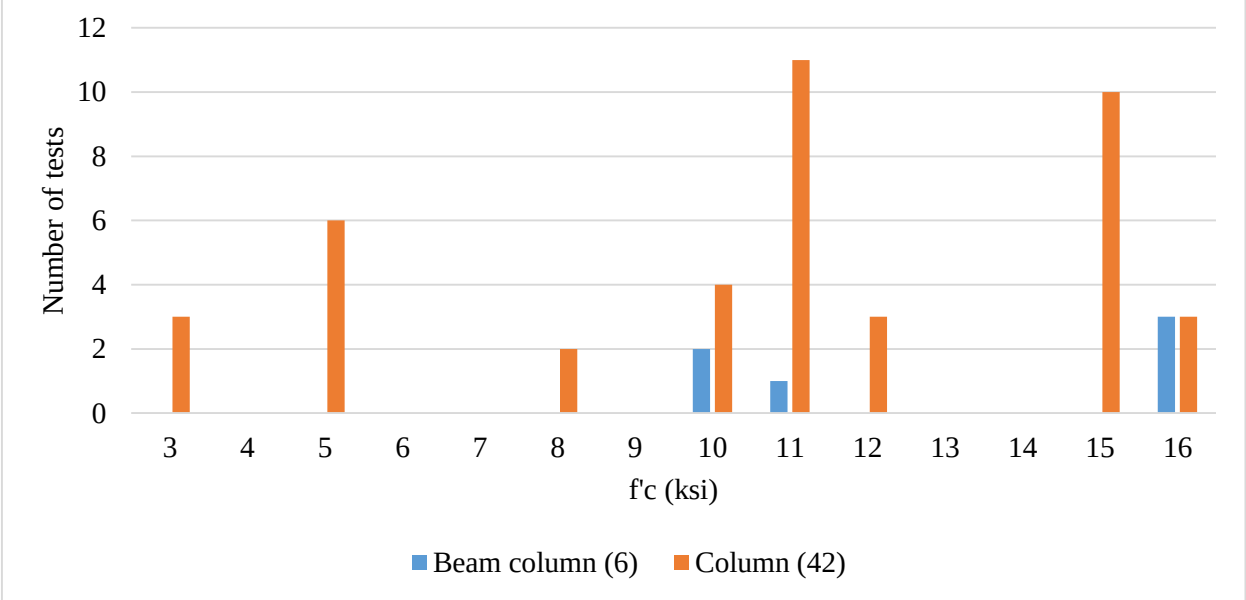

Figure A.4 Frequency distribution of f_c' for CCFT column database failing in local buckling

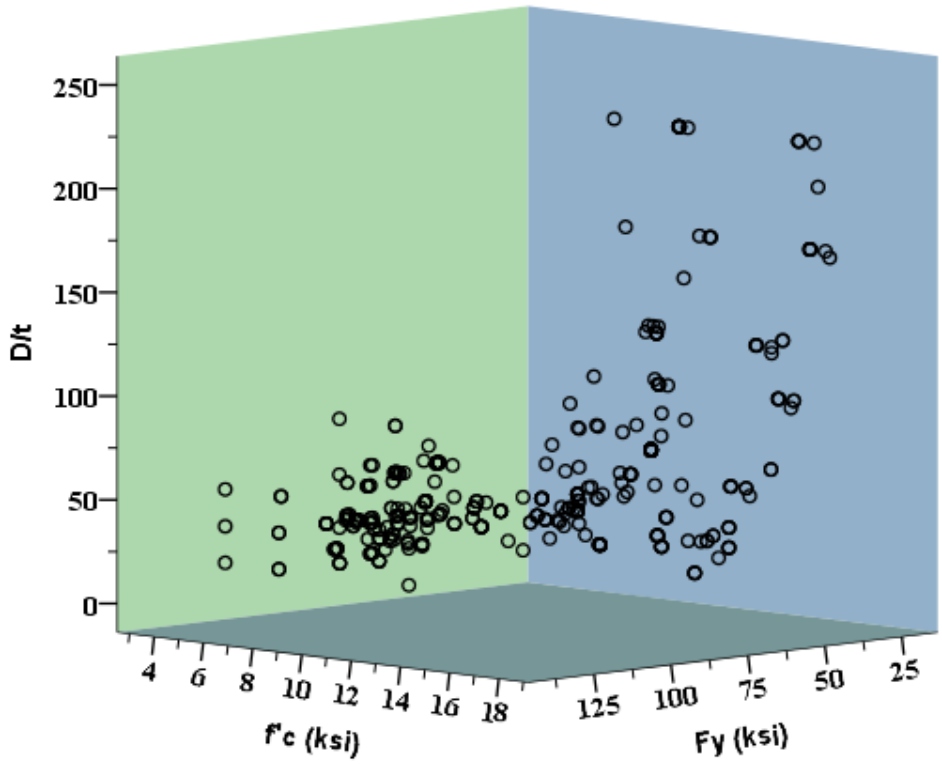

Figure A.5 Database of all CCFT member tests

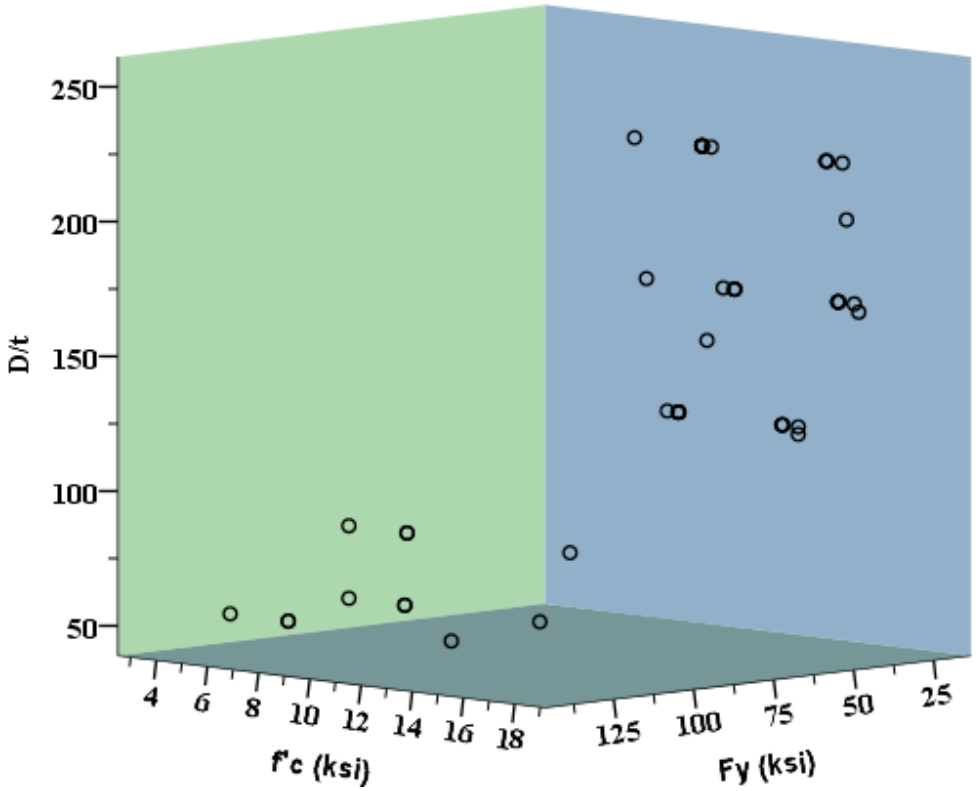

Figure A.6 Database of CCFT members failing in local buckling

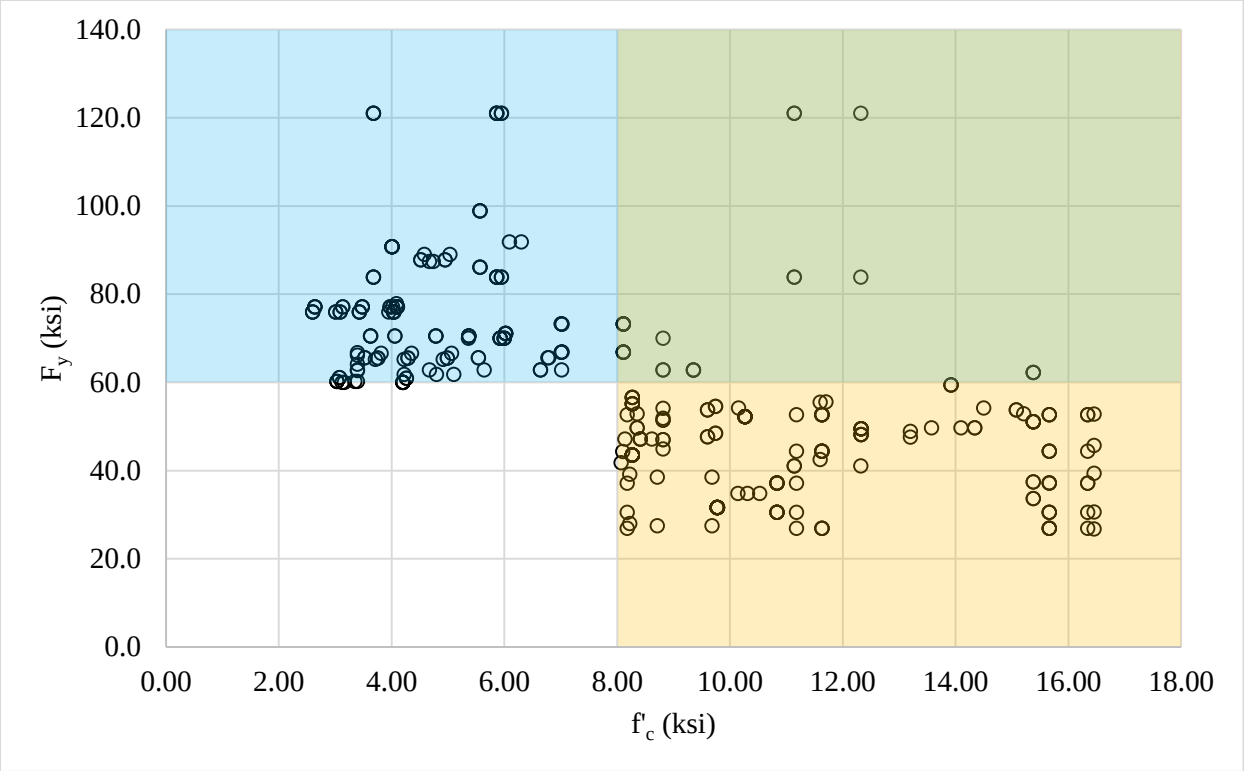

Figure A.7 Database available for CCFT members

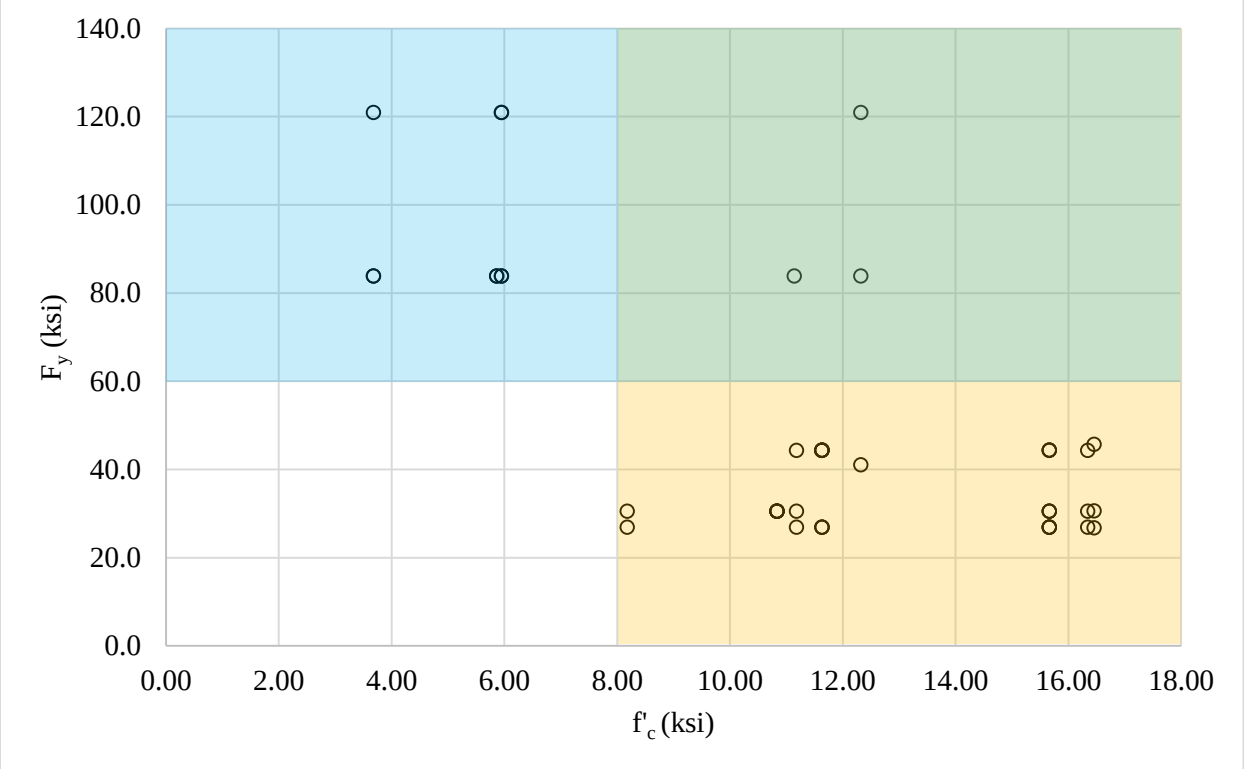

Figure A.8 Database available for CCFT members failing in local buckling

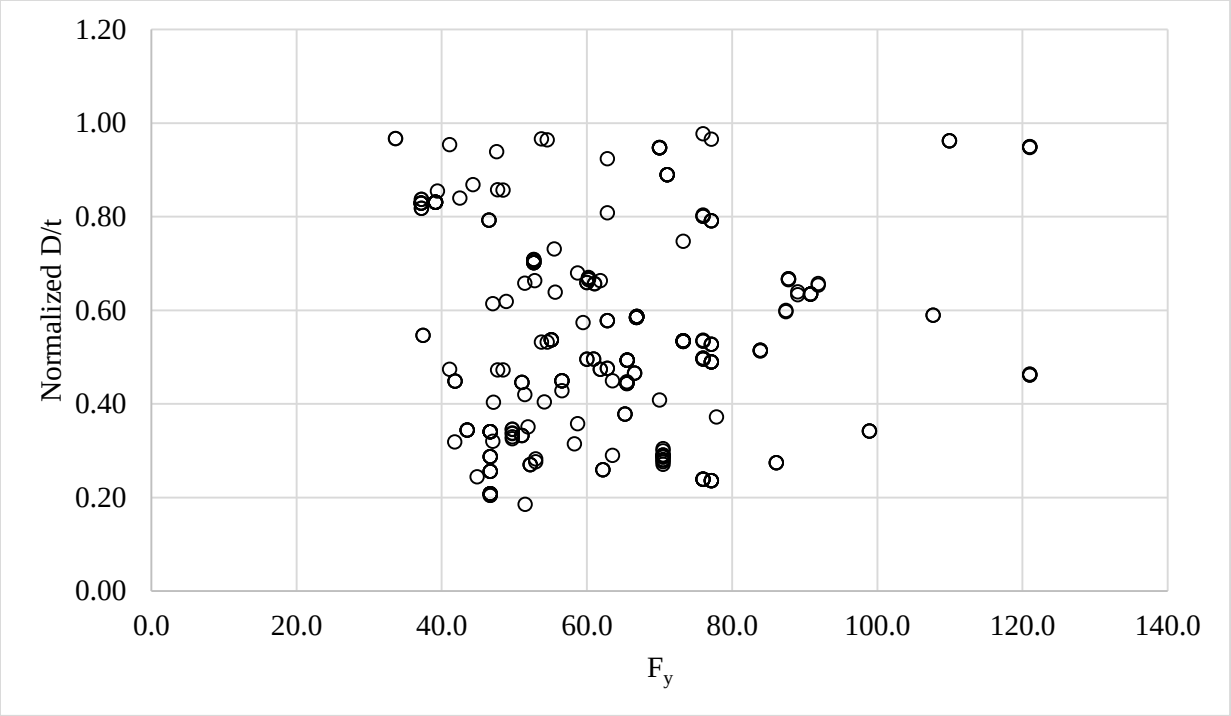

Figure A.9 CCFT Compact Column

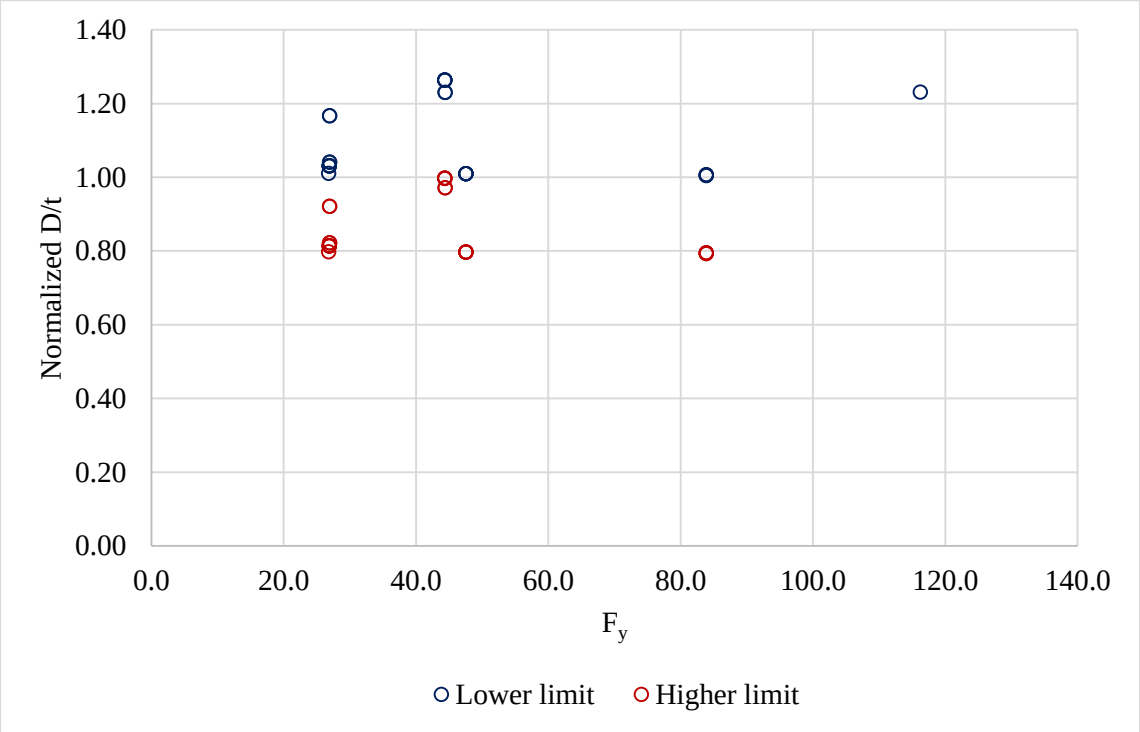

Figure A.10 CCFT non compact columns

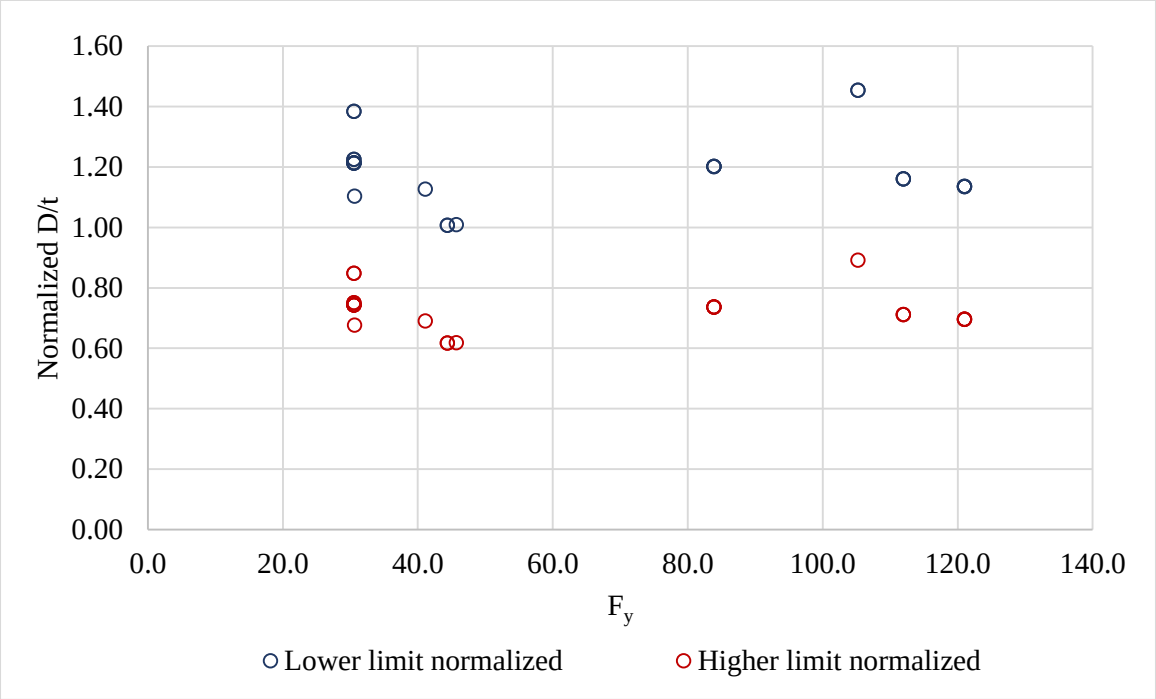

Figure A.11 CCFT slender columns

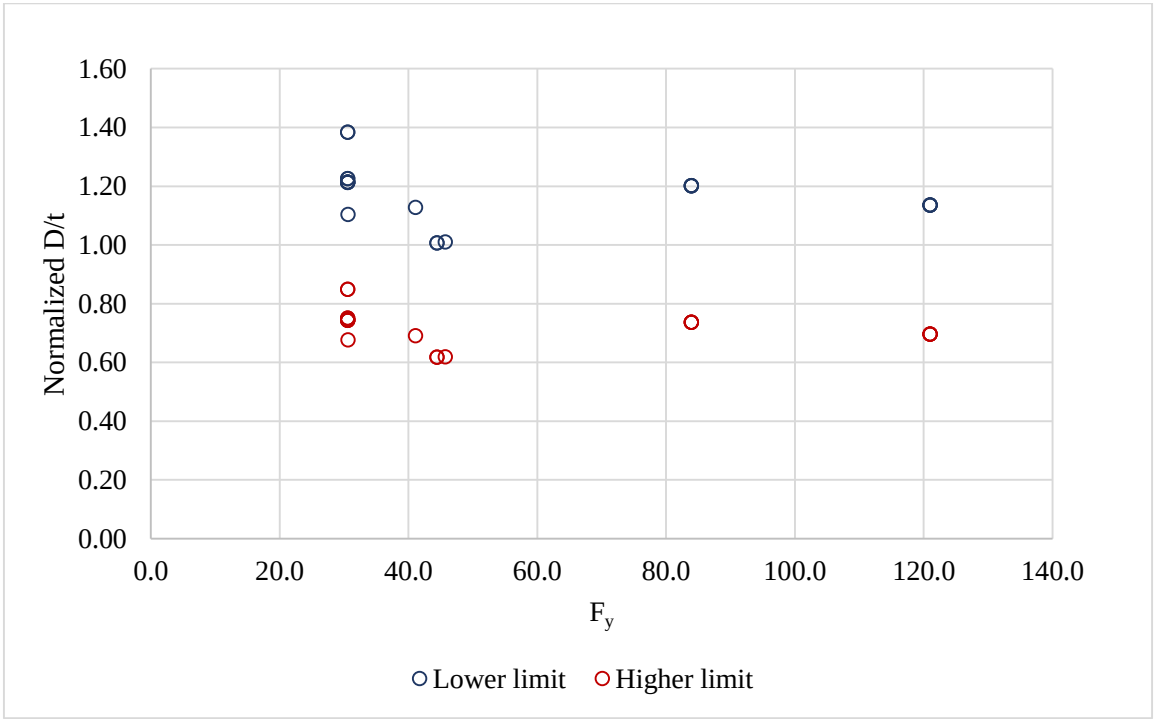

Figure A.12 CCFT slender columns failing in local buckling

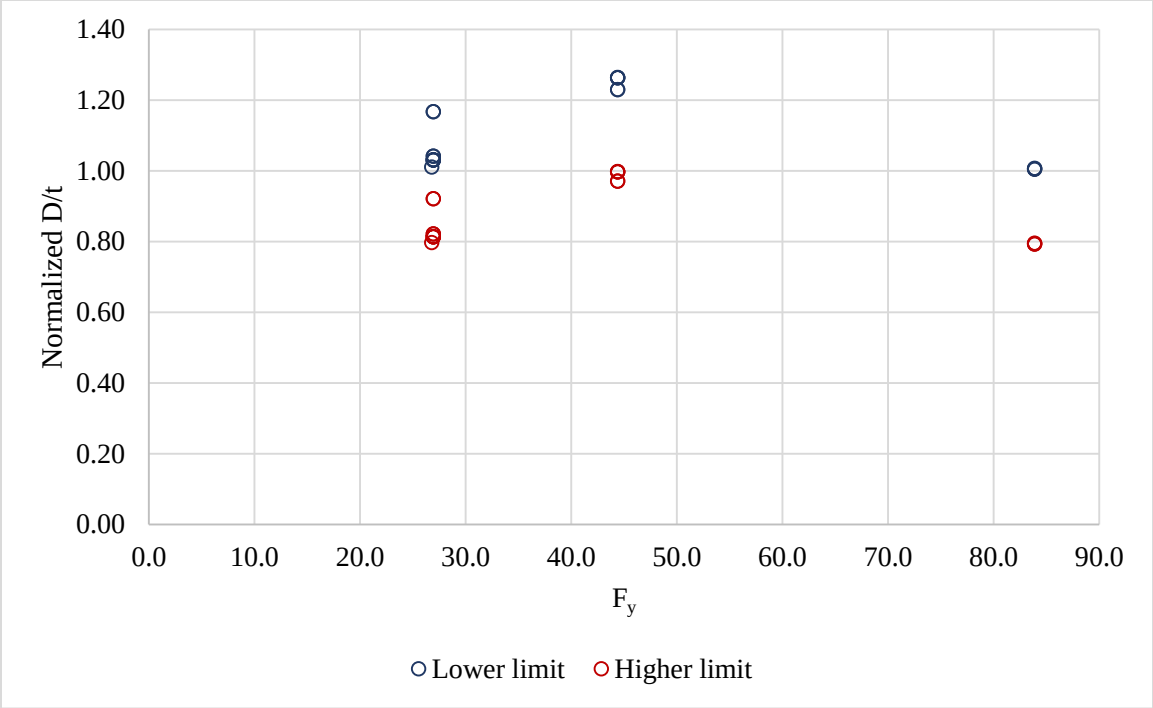

Figure A.13 CCFT non compact columns failing in local buckling

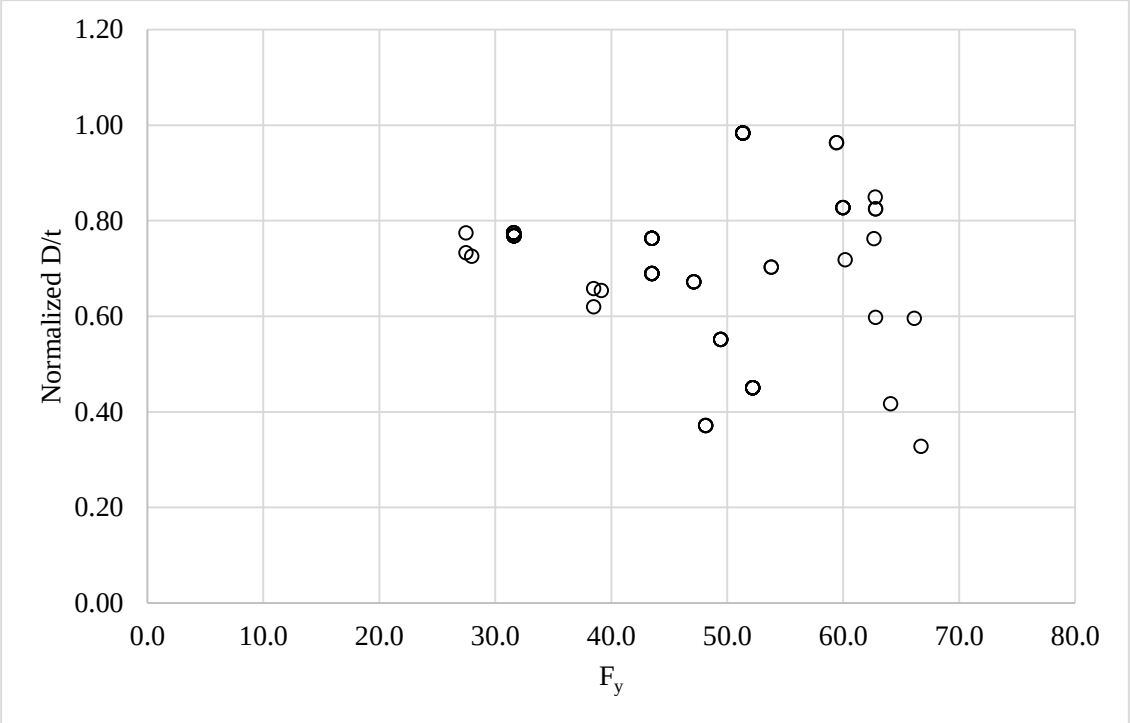

Figure A.14 CCFT Compact Beam Column

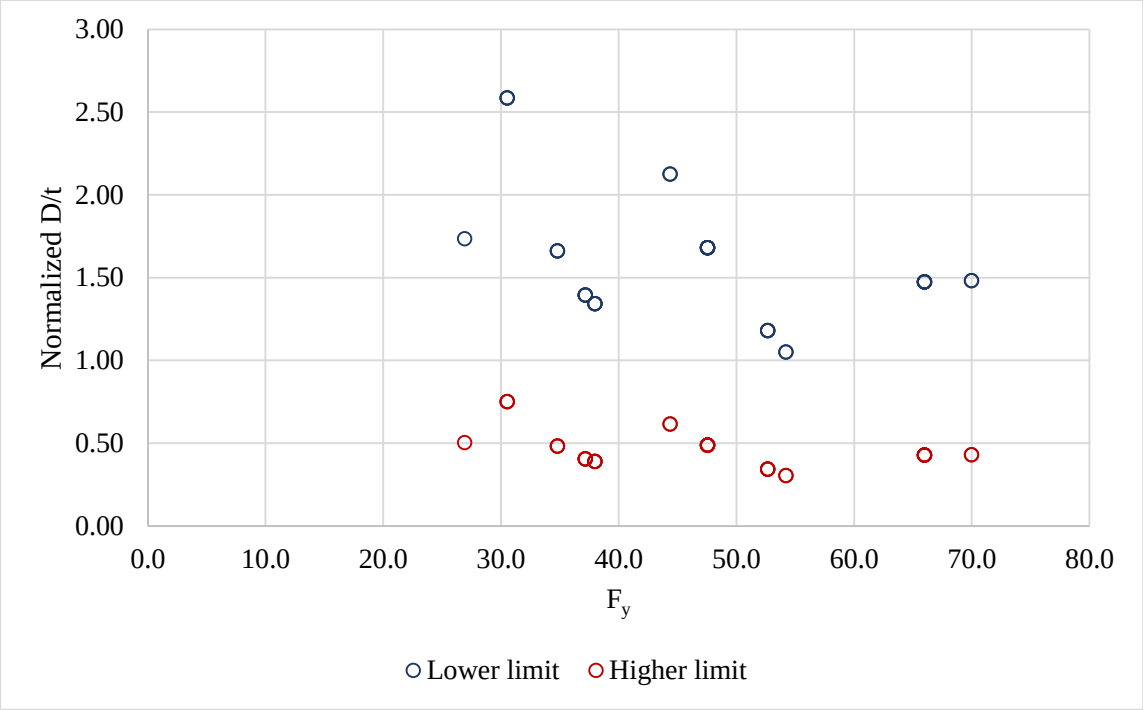

Figure A.15 CCFT non compact beam columns

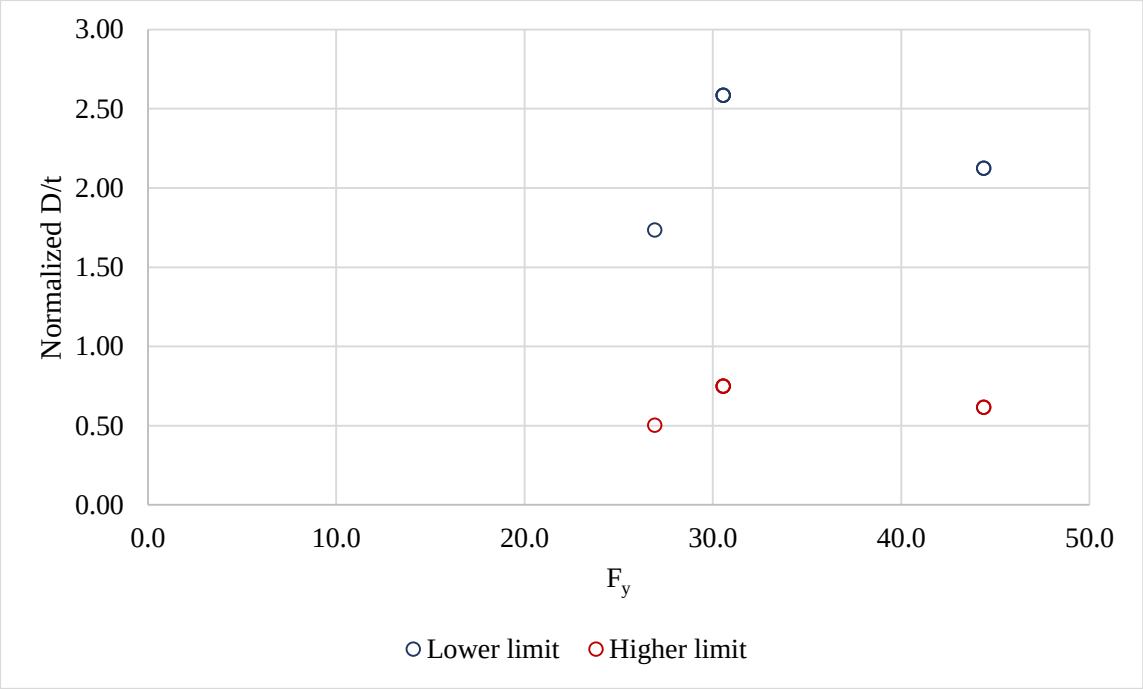

Figure A.16 CCFT non compact beam columns failing in local buckling

APPENDIX B.1 COUPON TESTING

The typical tensile testing coupon specimen are cut in the profile as shown in Figure B.1.1 from the metal sheets. The testing procedure is followed as per ASTM E8-15a.

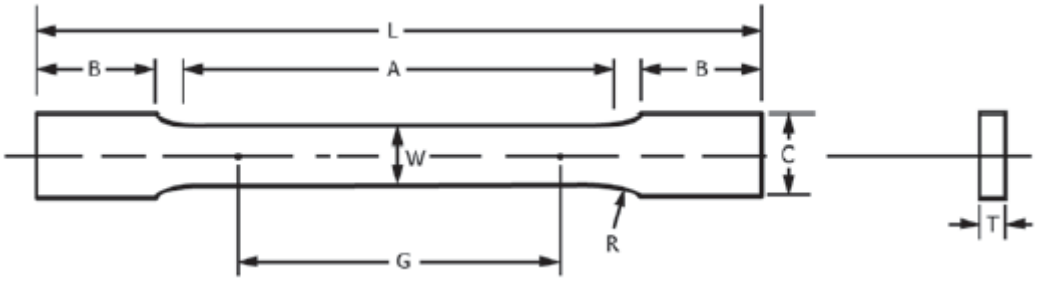

Figure B.1. 1 Rectangular tensile testing specimen (ASTM E8-15a)

Table B.1. 1 Tensile coupon dimensions

Dimensions	
	Sheet-Type, 12.5 mm (0.5 in.) wide mm (in.)
G – Gauge length	50.0 ± 0.1 (2.00 ± 0.005)
W – Width	12.5 ± 0.2 (0.500 ± 0.010)
T – Thickness	varying
R – Radius of fillet, min	12.5 (0.5)
L – Overall length, min	200 (8)
A – Length of reduced section, min	57 (2.25)
B – Length of grip section, min	50 (2)
C – Width of grip section, approximate	20 (0.75)

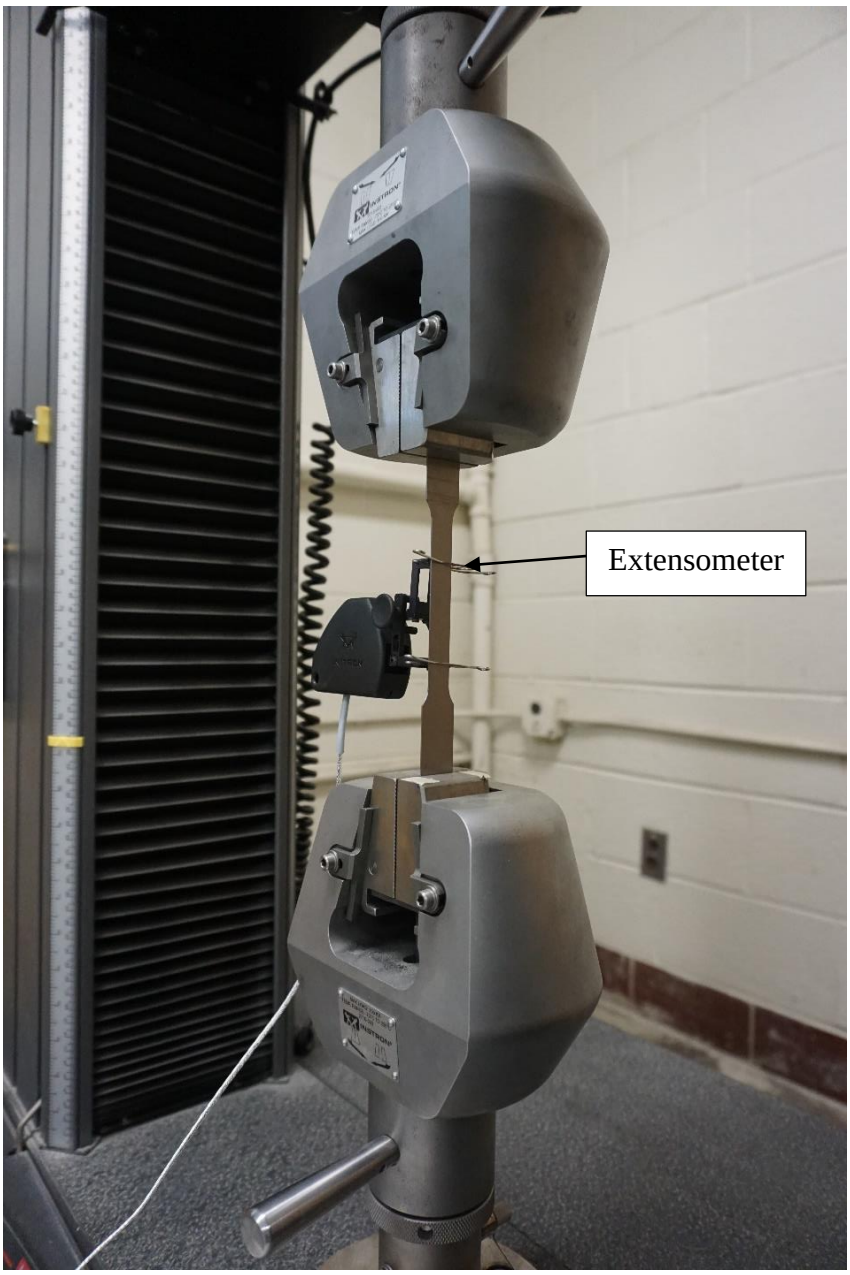

Figure B.1. 2 Coupon testing set up

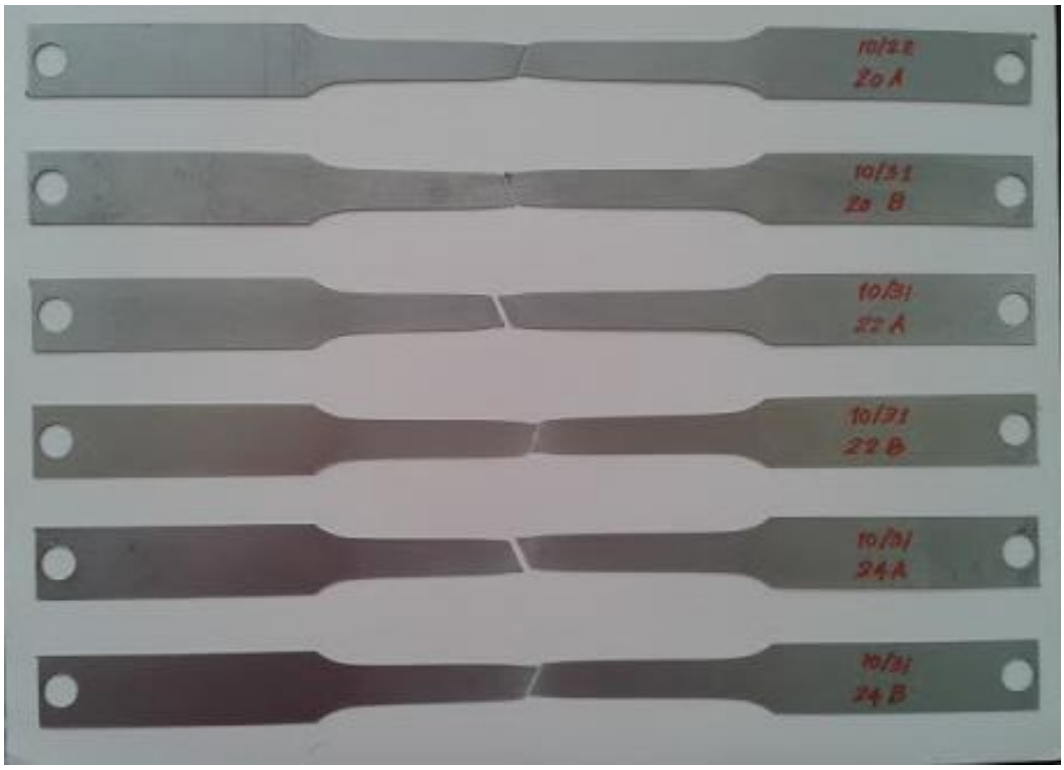

Figure B.1. 3 Coupon testing specimen failure

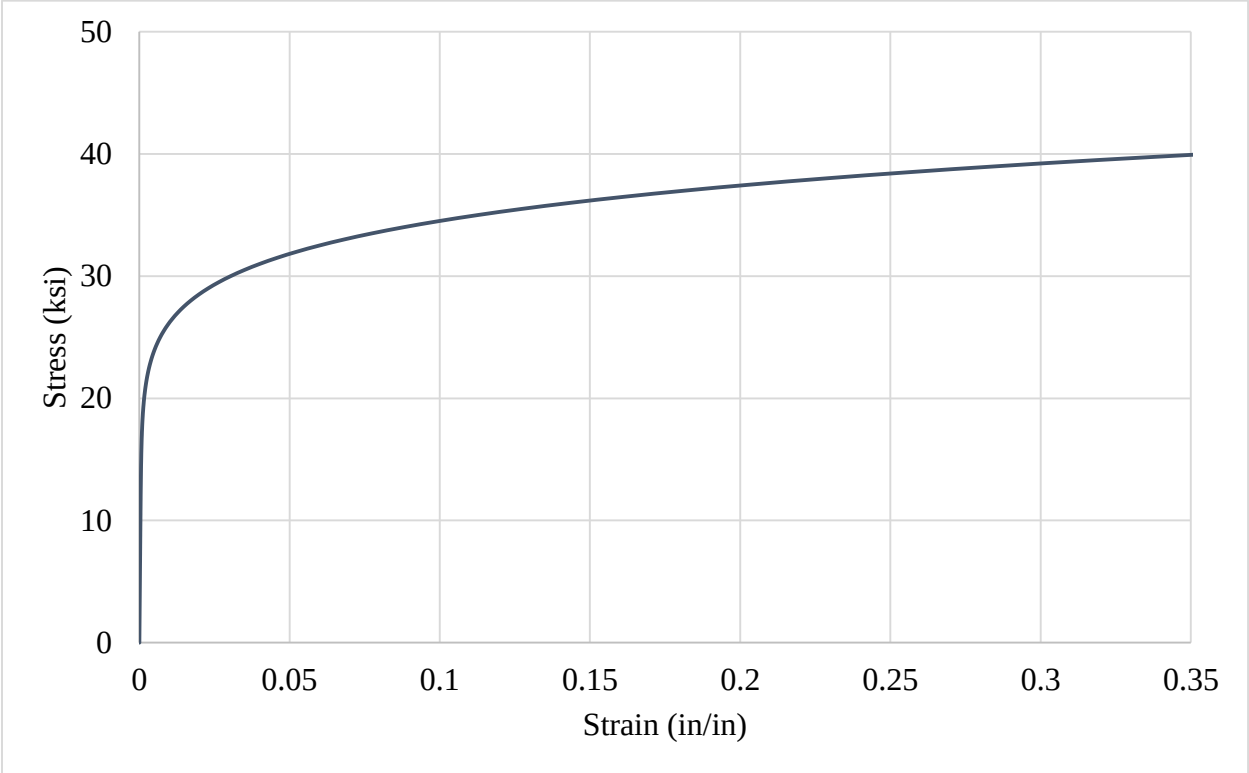

Figure B.1. 4 Ramberg-Osgood curve for steel used in the experiment

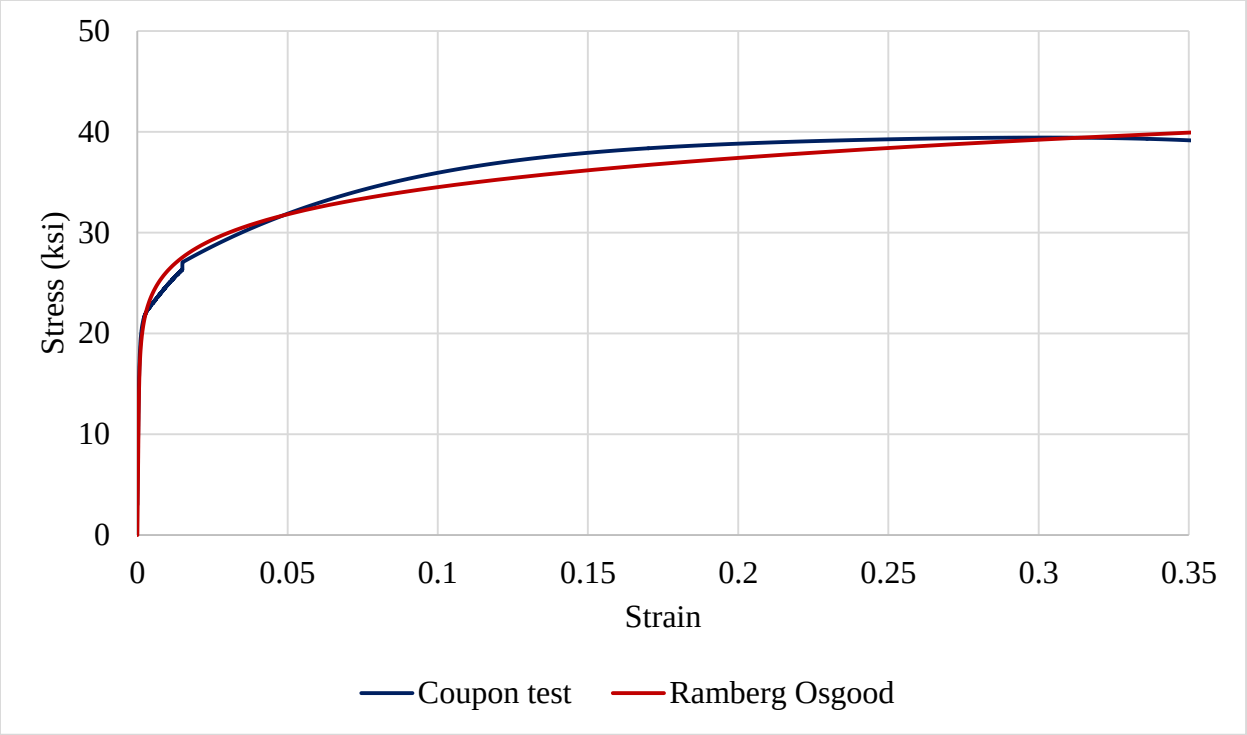

Figure B.1. 5 Comparison between Ramberg-Osgood curve and coupon test result

APPENDIX B.2 INFILL CONCRETE

Table B.2. 1 Concrete mix design used for 7 ksi concrete

Concrete Mix	Required compressive strength : 7000 psi		at 28 days
Concrete ingredients	Weight	Density	volume
Portland Cement	564 lbs.	94 lb/ft^3	6 ft^3
Fine aggregates	1350 lbs.	100 lb/ft^3	13.5 ft^3
Coarse aggregates	1750 lbs.	150 lb/ft^3	11.67 ft^3
Water	282 lbs	62.5 lb/ft^3	4.5 ft^3
Entrapped air content	3.0%		1.07 ft^3
Total volume of the concrete obtained			36.74 ft^3
Water-Cement ratio		0.50	

Table B.2. 2 Compressive strength of the infill concrete

Cylinder No.	**Load (kips)**	**Compressive strength (ksi)**
1	93.210	7.417
2	89.565	7.127
3	90.040	7.165
4	91.755	7.302
5	87.725	6.981
6	94.210	7.497
7	91.010	7.242
8	87.325	6.949
9	87.225	6.941
10	86.030	6.846
Average compressive strength		7.147

APPENDIX B.3 TEST SETUP

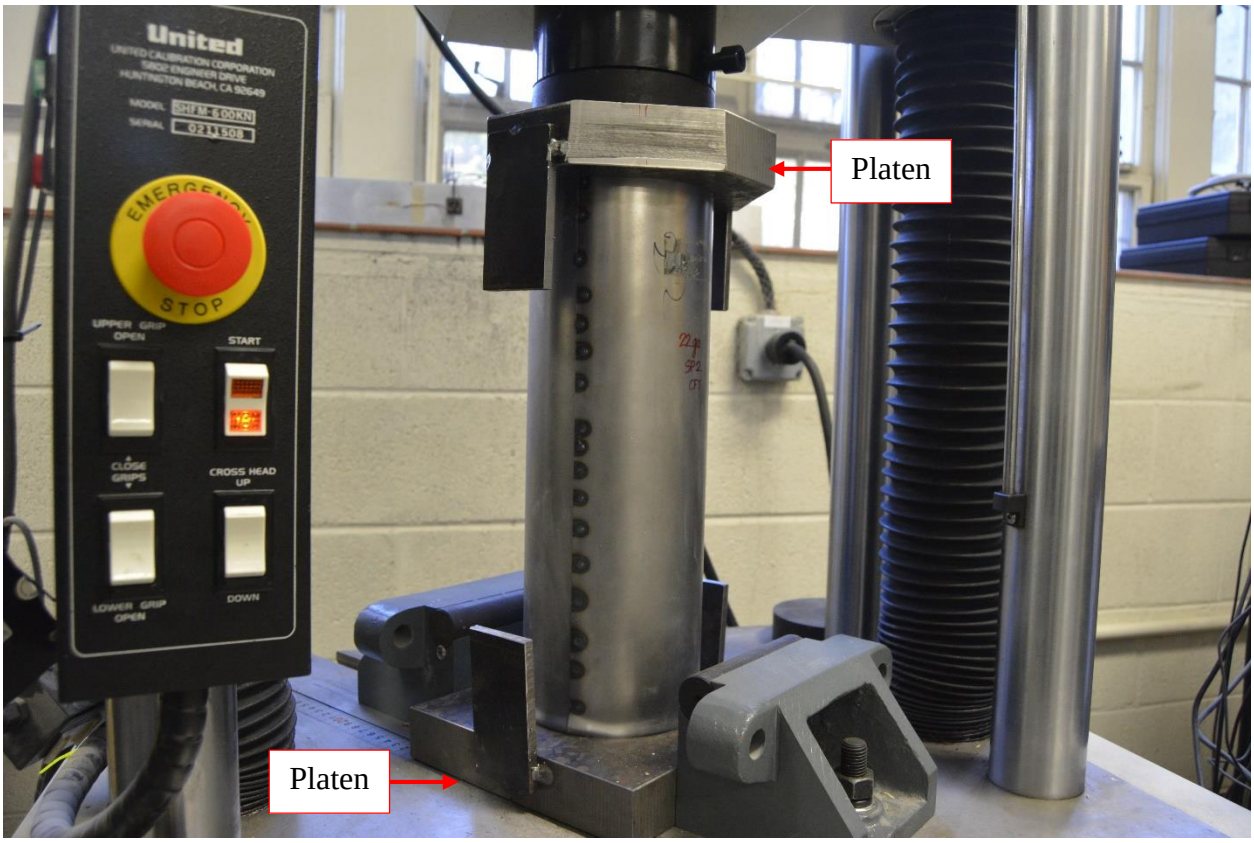

Figure B.3. 1 Typical test setup for axial compression testing

APPENDIX C. HOLLOW TUBE TESTING

Figure C.1 Local buckling of 20 ga hollow tube (Specimen 1)

Figure C.2 Local buckling of 20 ga hollow tube (Specimen 2)

Figure C.3 Local buckling of 22 ga hollow tube (Specimen 1)

Figure C.4 Local buckling of 22 ga hollow tube (Specimen 2)

Figure C.5 Local buckling of 22 ga hollow tube (Specimen 3)

Figure C.6 Local buckling of 22 ga hollow tube (Specimen 4)

Figure C.7 Local buckling of 26 ga hollow tube (Specimen 1)

Figure C.8 Local buckling of 26 ga hollow tube (Specimen 2)

APPENDIX D.1. CONCRETE FILLED TUBE TESTING (TYPE I)

Figure D.1.1 Local buckling of 20 ga concrete filled tube (Specimen 1)

Figure D.1.2 Local buckling of 22 ga concrete filled tube (Specimen 1)

Figure D.1.3 Local buckling of 26 ga concrete filled tube (Specimen 1)

APPENDIX D.2. CONCRETE FILLED TUBE TESTING (TYPE II)

Figure D.2.1 Local buckling of 20 ga concrete filled tube (Specimen 2)

Figure D.2.2 Local buckling of 20 ga concrete filled tube (Specimen 3)

Figure D.2.3 Local buckling of 22 ga concrete filled tube (Specimen 2)

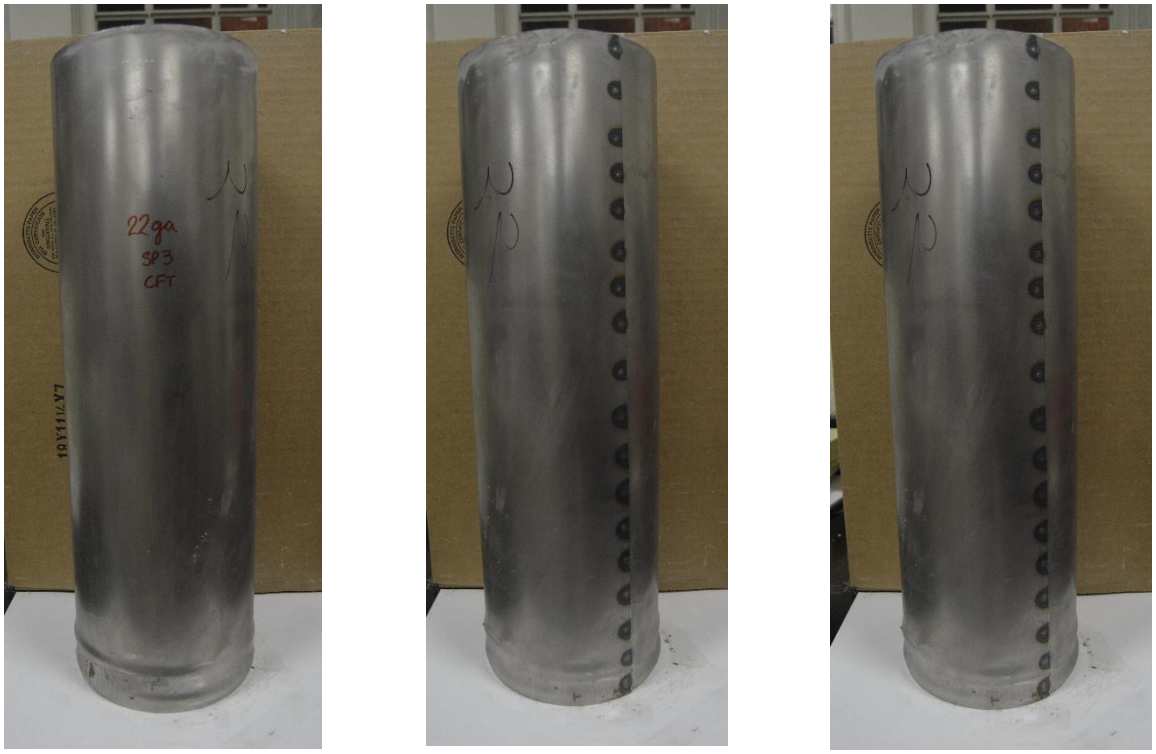

Figure D.2.4 Local buckling of 22 ga concrete filled tube (Specimen 3)

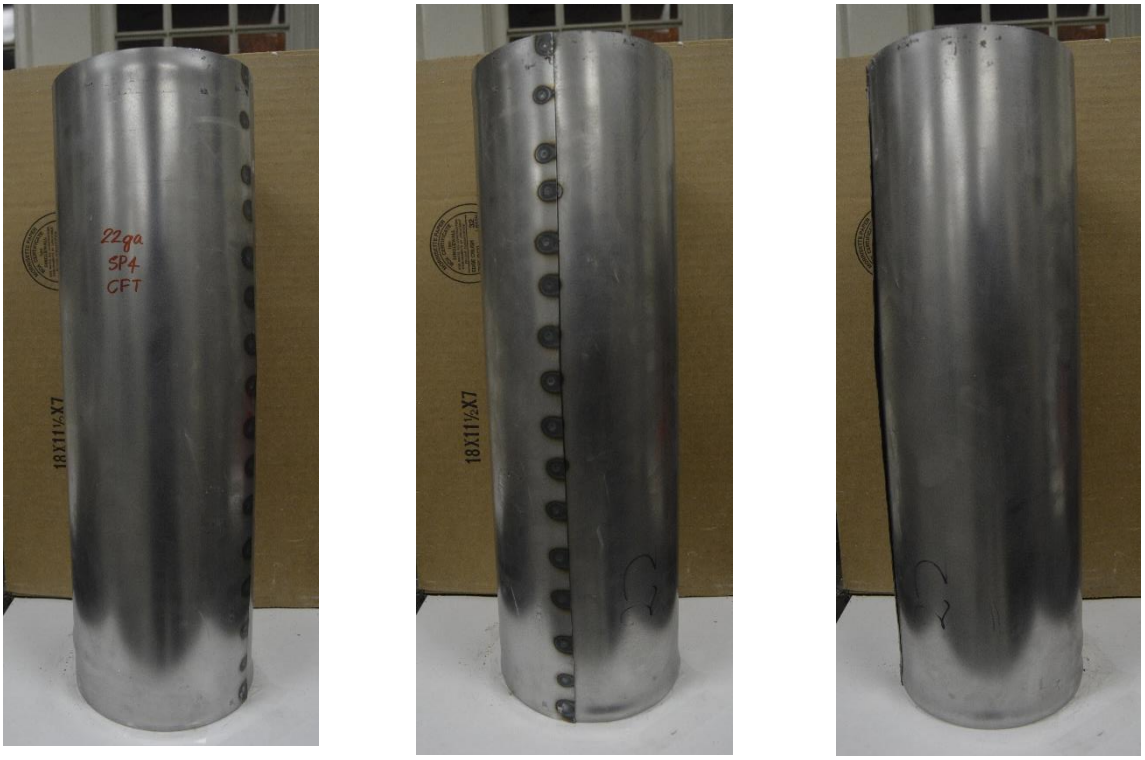

Figure D.2.5 Local buckling of 22 ga concrete filled tube (Specimen 4)

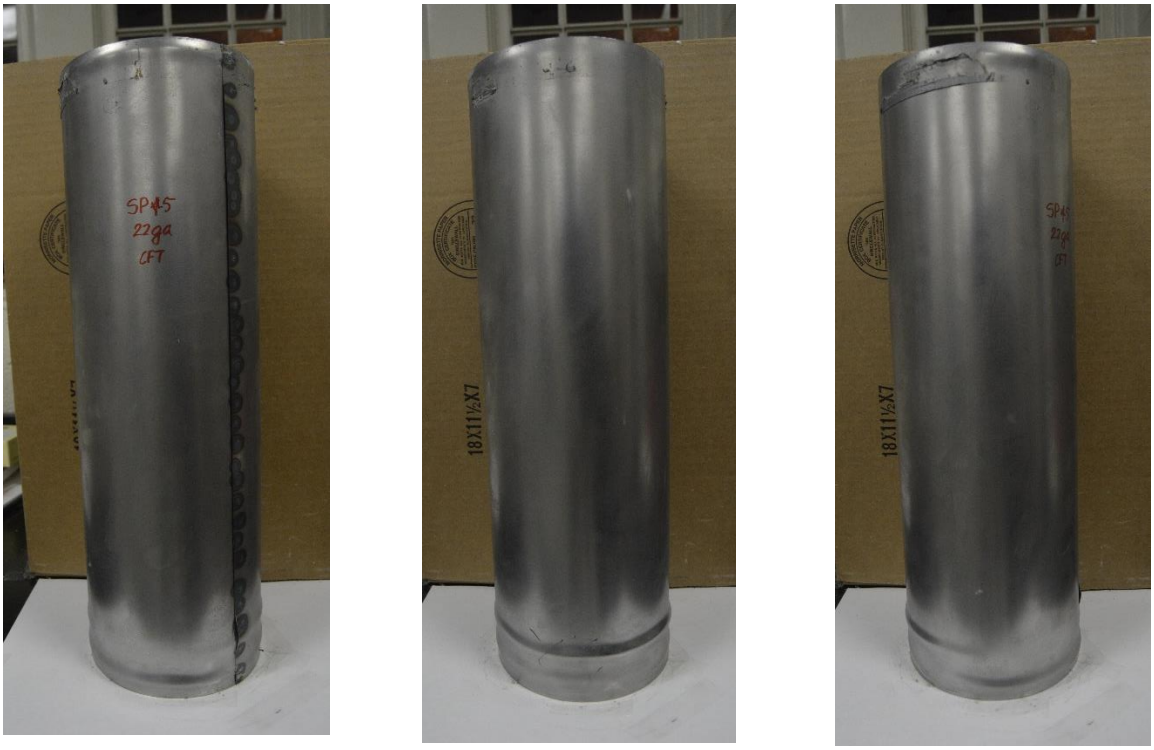

Figure D.2.6 Local buckling of 22 ga concrete filled tube (Specimen 5)

Figure D.2.7 Local buckling of 22 ga concrete filled tube (Specimen 6)

Figure D.2.8 Local buckling of 26 ga concrete filled tube (Specimen 2)

Figure D.2.9 Local buckling of 26 ga concrete filled tube (Specimen 3)

REFERENCES

ASTM E8/E8M-15a Standard Test Method for Tension Testing of Metallic Materials

Zhang, J. (2009). Elastic/plastic buckling of cylindrical shells with elastic core under axial compression. Thesis, McGill University, Canada.

Bradford, M. A., Loh, H. Y., & Uy, B. (2002). Slenderness limits for filled circular steel tubes. *Journal of Constructional Steel Research*, *58*(2), 243-252.

Bradford, M. A., Roufegarinejad, A., & Vrcelj, Z. (2006). Elastic buckling of thin-walled circular tubes containing an elastic infill. *International Journal of Structural Stability and Dynamics*, *6*(04), 457-474.

Timoshenko, S. P., & Gere, J. M. (2009). *Theory of elastic stability*. Courier Corporation.

Lee, L. H. (2012). Inelastic buckling of initially imperfect cylindrical shells subject to axial compression. *Journal of the Aerospace Sciences*.

Sakino, K., Nakahara, H., Morino, S., & Nishiyama, I. (2004). Behavior of centrally loaded concrete-filled steel-tube short columns. *Journal of Structural Engineering*, *130*(2), 180-188.

Ellobody, E., Young, B., & Lam, D. (2006). Behaviour of normal and high strength concrete-filled compact steel tube circular stub columns. *Journal of Constructional Steel Research*, *62*(7), 706-715.

Liang, Q. Q. (2009). Strength and ductility of high strength concrete-filled steel tubular beam–columns. *Journal of Constructional Steel Research*, 65(3), 687-698.

Liang, Q. Q. (2011). *High strength circular concrete-filled steel tubular slender beam–columns, Part I: Numerical analysis*. *Journal of Constructional Steel Research*, 67(2), 164-171.

Liang, Q. Q. (2011). High strength circular concrete-filled steel tubular slender beam–columns, Part II: Fundamental behavior. *Journal of Constructional Steel Research*, 67(2), 172-180.

Morino, S. (2000). Recent Developments on CFT Column Systems: US-Japan Cooperative Earthquake Research Program.

O'shea, M., & Bridge, R. (1997). The Design for local buckling of concrete filled steel tubes. In Composite construction-conventional and innovative. *International conference* (pp. 319-324).

O'Shea, M. D., & Bridge, R. Q. (1994, December). High strength concrete in thin-walled circular steel sections. In *Proceedings of the 6th International Symposium on Tubular Structures* (pp. 277-284).

Portolés, J. M., Romero, M. L., Bonet, J. L., & Filippou, F. C. (2011). Experimental study of high strength concrete-filled circular tubular columns under eccentric loading. *Journal of constructional steel research*, 67(4), 623-633.

Prion, H. G., & Boehme, J. (1994). Beam-column behaviour of steel tubes filled with high strength concrete. *Canadian Journal of Civil Engineering*, 21(2), 207-218.

Saisho, M., & Mitsunari, K. (1992). Dynamic restoring force characteristics of steel tube filled with super-high strength concrete. *Earthquake Engineer 10th World*, *6*, 3201.

Varma, A. H., Ricles, J. M., Sause, R., & Lu, L. W. (2002). Seismic behavior and modeling of high-strength composite concrete-filled steel tube (CFT) beam–columns. *Journal of Constructional Steel Research*, 58(5), 725-758.

Varma, A. H., Ricles, J. M., Sause, R., Ream, A., & Lu, L. W. (2004). Seismic Performance of High Strength CFT Beam-Columns. In *Advanced Technology in Structural Engineering* (pp. 1-8). ASCE.

Varma, A. H., Ricles, J. M., Sause, R., & Lu, L. W. (2004). Seismic behavior and design of high-strength square concrete-filled steel tube beam columns. *Journal of Structural Engineering*, 130(2), 169-179.

Yamamoto, T., Kawaguchi, J., & Morino, S. (2000). Experimental study of scale effects on the compressive behavior of short concrete-filled steel tube columns. In *Proceedings of the united engineering foundation conference on composite construction in steel and concrete IV (AICE).* Banff, Canada (pp. 879-91).

Zhang, S., & Guo, L. (2007). Behaviour of high strength concrete-filled slender RHS steel tubes. *Advances in Structural Engineering*, 10(4), 337-351.

Leon, R. T., & Aho, M. F. (2002). Towards new design provisions for composite columns. *Composite Construction in Steel and Concrete IV*, 518-527.

Schneider, S. P. (1998). Axially loaded concrete-filled steel tubes. *Journal of structural Engineering*, 124(10), 1125-1138.

Giakoumelis, G., & Lam, D. (2004). Axial capacity of circular concrete-filled tube columns. *Journal of Constructional Steel Research*, *60*(7), 1049-1068.

Mander, J. B., Priestley, M. J., & Park, R. (1988). Theoretical stress-strain model for confined concrete. *Journal of structural engineering*, *114*(8), 1804-1826.

Sakino, K., Nakahara, H., Morino, S., & Nishiyama, I. (2004). Behavior of centrally loaded concrete-filled steel-tube short columns. *Journal of Structural Engineering*, *130*(2), 180-188.

O'Shea, M. D., & Bridge, R. Q. (2000). Design of circular thin-walled concrete filled steel tubes. *Journal of Structural Engineering*, *126*(11), 1295-1303.

Lam, D., & Gardner, L. (2008). Structural design of stainless steel concrete filled columns. *Journal of Constructional Steel Research*, *64*(11), 1275-1282.

Lee, J., & Fenves, G. L. (1998). Plastic-damage model for cyclic loading of concrete structures. *Journal of engineering mechanics*, *124*(8), 892-900.

Kupfer, H., Hilsdorf, H. K., & Rusch, H. (1969, August). Behavior of concrete under biaxial stresses. In *Journal Proceedings* (Vol. 66, No. 8, pp. 656-666).

Bazant, Z. P., & Jirásek, M. (2002). Nonlocal integral formulations of plasticity and damage: survey of progress. *Journal of Engineering Mechanics*, *128*(11), 1119-1149.

AISC (2010). Specification for Structural Steel Buildings (ANSI/AISC 360-10). *American Institute of Steel Construction,* Chicago-Illinois.

ACI-318 (2014). Building Code Requirements for Structural Concrete and Commentary

ABAQUS. (6.14-4), *ABAQUS FEA*. SIMULIA. ABAQUS Inc.

Ramberg, W., & Osgood, W. R. (1943). Description of stress-strain curves by three parameters.

Chen, W. F., & Han, D. J. (2007). *Plasticity for structural engineers*. J. Ross Publishing.